Investigation of buckling characteristics of cracked variable stiffness composite plates by an eXtended Ritz approach

A. Milazzo[a], V. Oliveri[b]

[a] *Department of Engineering,University of Palermo, Viale delle Scienze, Bldg 8, 90128 Palermo - Italy*
[b] *Bernal Institute, School of Engineering, University of Limerick, Limerick, Ireland*

Abstract

Variable Angle Tow (VAT) composite plates are characterized by in-plane variable stiffness properties, which opens to new concepts of stiffness tailoring and optimization to achieve higher structural performance for advanced lightweight structures where damage tolerance consideration are often mandatory. In this paper, a single-domain eXtended Ritz formulation is proposed to study the buckling behaviour of variable stiffness laminated cracked plates. The plate behavior is described by the first order shear deformation theory whose generalized displacements, namely reference plane translations and rotations, are expressed via suitable admissible trial functions.These consist of a set regular terms, built using orthogonal polynomials, augmented with special functions able to describe the crack opening and the singular behaviour at the crack tips; boundary functions are used to ensure the required homogeneous essential boundary conditions. Governing equations are inferred via the principle of virtual displacements an solved to carry out an extensive study on the buckling behaviour of variable angle tow homogeneous and layered composite plates. The results obtained for homogeneous plates evidence that the crack presence strongly influences the buckling behaviour depending on its length and inclination and plate boundary conditions with a meaningful variability with respect to the fibre paths configuration, which can arrange for better performances with respect to the straight fiber case. Also for cracked laminates the results show that there are several fibre path able to provide higher buckling loads and higher overall axial stiffness with respect to the straight fibre case. In the framework of damage tolerant engineering applications, this allows to select fibre paths that guarantee predefined design levels of buckling load and axial stiffness even in presence of cracks. Finally, this study highlights the potential of the proposed approach for the analysis of the buckling behaviour of cracked composite variable stiffness plates, which provides an efficient analysis tool for the damage tolerant design and

Email addresses: alberto.milazzo@unipa.it (A. Milazzo), vincenzo.oliveri@ul.ie (V. Oliveri)

optimization of advanced VAT structures.

Keywords: Extended Ritz method, X-Ritz, variable stiffness, cracked plates, buckling

---

1. Introduction

Structural performances and efficiency have been meaningfully improved by the introduction of fiber-reinforced composite materials. Their high strength-to weight and stiffness-to-weight ratios, combined with the constituent material selection and the application in the form of optimized layup laminate configurations, made possible to achieve structural design tailored to the application. The first generation of composite structures for aerospace, automotive and naval engineering applications has been based on the available production technologies and was implemented using laminates built with straight fibres plies; this leads to build plate and shell structures exhibiting constant stiffness across their reference surface. Indeed, the concept of variable stiffness added a further dimension to the structural design space providing an increased freedom to tailor the structural behaviour. In this context, the growth of a reliable industrial automation and the availability of automated fiber placement manufacturing methods led towards the introduction of in-plane variable stiffness composites, generally known as variable angle tow (VAT) composites [1, 2]. In these composites the fiber orientation is point-wise varied by actively steering individual fibre tows rather than place them along constant directions. By doing so, two dimensional structures (plates and shells) with continuously varying in-plane properties and discretely varying through-thickness properties are obtained. It is worth noting that this class of structures conceptually differs from usually defined functionally graded composites, which exhibit only continuously varying through-thickness properties and constant stiffnesses across the structural reference surface. The employment of variable stiffness structures in engineering applications, especially in the form of high performance VAT components, requires accurate analyses for assessing their static, dynamic, fatigue and damage tolerance behaviour and for carrying out the ensuing optimized design. Considering the involved complexity (variable anisotropy and heterogeneity), the variable stiffness composites models should simultaneously be able to accurately capture the structural responses and do this efficiently in order to be acknowledged as tools for a reliable, effective and safe design.

With this background in mind, the Ritz method has proven to be a successful and accurate approach for the analysis of composite plates with high computational efficiency [3–7]. Ritz solutions for linear static, free vibrations, buckling and postbuckling analysis of straight fibers composite plates,

frequently implementing the classical laminated plate theory (CLPT) (e.g. [8–13]), have been proposed. As transverse shear strains can play an important role in composite structures, the first-order shear deformation theory (FSDT) is advised as adequate for the engineering analysis and design of most thin to moderately thick composite laminates [5] and it is appealing when compared with more sophisticated higher order plate theories due to its simplicity and low computational costs. Focusing on FSDT modelling of straight fibers plates solved by the Ritz method, formulation based on different kinds of trial function have been proposed, showing reliable results for static [14, 15], free vibrations [16–21], buckling [16, 14] and postbuckling [22–24] analysis. Regarding variable stiffness composite structures and VAT composites, attention has been devoted to both CLPT [25–36] and FSDT [37–41] modelling of plates and shells.

In high performance lightweight structures the presence of cracks can severely affect the load carrying capability and such damages together with their related effects need to be accounted for fail safe or damage tolerant design. Attention should be also devoted to the buckling and post-buckling behaviour of cracked plates as unexpected critical safety issues could manifest [42]. The Ritz method has been used to analyze cracked plates and approaches based on the decomposition technique [43–48] have been implemented providing sound results that however does not explicitly consider the crack tip singular behaviour. To cope this issue, single-domain Ritz formulations have been introduced that employ special trial functions able to describe the discontinuous behaviour across the crack as well as the crack tip singular stresses [49–62]. The literature survey reveals that no solution for cracked variable stiffness plate has been yet presented and that no results are available to show the crack effects on the behaviour of such structures.

With the intent of filling this gap and grounding on their previous works [60–62], in the present paper the authors extend to the analysis of variable stiffness plates a single-domain Ritz formulation, named X-Ritz, which inherently accounts for embedded or edge crack presence. The plate model is based on a first-order shear deformation theory where the primary variables are expressed as combination of orthogonal polynomials and set of suitable trial functions able to represent crack discontinuity and singular behaviour. The aim of this work is (i) to verify the applicability of the approach to variable stiffness structures, and (ii) to study the effects of cracks on the behaviour of VAT plates, focussing the attention on their influence on the plates' buckling behaviour. To the best of the authors' knowledge this is the first study proposed in the literature that accounts for crack damages in VAT plates and the presented original results can serve as benchmark for future works.

The work is organised as follow: the cracked plate formulation and details of the X-Ritz approximation procedure are presented in Sec.2. Next, the validation of the proposed method and original results are discussed in Sec.3, followed by concluding remarks in Sec.4.

2. Formulation

Consider a general quadrilateral plate containing a straight embedded or edge through-the-thickness crack. As shown in Fig.1, the plate is referred to a Cartesian coordinate system $O\{x_1, x_2, x_3\}$ with the x_3 axis directed along the thickness and the x_1 and x_2 axes lying in the plate reference plane Ω whose boundary is denoted by $\partial\Omega$. A natural coordinate system $O\{\xi, \eta\}$ is also introduced, which maps the square domain $[-1, 1]\times[-1, 1]$ into the plate reference plane coordinates via standard bilinear shape functions [46]. The plate can be either homogeneous or layered and it generally exhibits stiffnesses variable across the reference plane related to the distribution of material properties (e.g. variable angle tow composites) or thickness. For layered plates, perfect bonding is assumed between contiguous plies. The plate is loaded by a system of loadings that determine an equilibrated pre-buckling state.

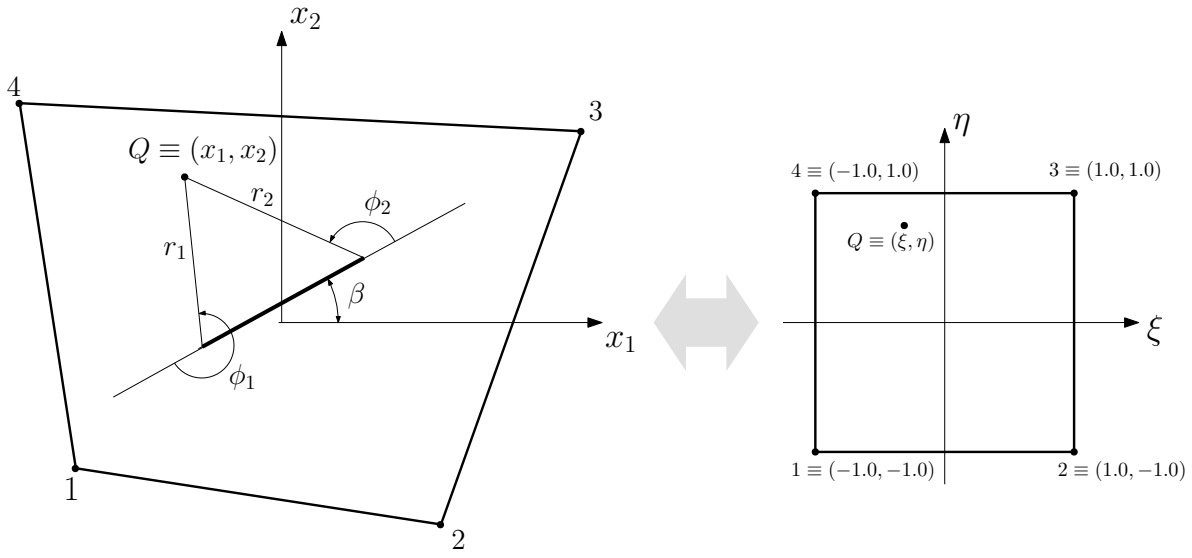

Figure 1: Plate geometry and reference systems.

According to the first order shear deformation theory [46], assuming that homogeneous essential boundary conditions on $\partial\Omega$ are satisfied, the plate buckling governing equations are obtained from the

stationarity conditions of the following functional

$$\Pi = \int_\Omega \frac{1}{2}\Big[(\boldsymbol{\mathscr{D}}_p \boldsymbol{u})^T \boldsymbol{A}\, \boldsymbol{\mathscr{D}}_p \boldsymbol{u} + (\boldsymbol{\mathscr{D}}_p \boldsymbol{u})^T \boldsymbol{B}\, \boldsymbol{\mathscr{D}}_p\, \boldsymbol{\mathscr{L}}\boldsymbol{\theta} + (\boldsymbol{\mathscr{D}}_p \boldsymbol{\mathscr{L}}\boldsymbol{\theta})^T \boldsymbol{B}\, \boldsymbol{\mathscr{D}}_p \boldsymbol{u} + (\boldsymbol{\mathscr{D}}_p \boldsymbol{\mathscr{L}}\boldsymbol{\theta})^T \boldsymbol{D}\, \boldsymbol{\mathscr{D}}_p \boldsymbol{\mathscr{L}}\boldsymbol{\theta} + (\boldsymbol{\mathscr{D}}_n \boldsymbol{u} + \boldsymbol{\mathscr{L}}\boldsymbol{\theta})^T \boldsymbol{S}\ (\boldsymbol{\mathscr{D}}_n \boldsymbol{u} + \boldsymbol{\mathscr{L}}\boldsymbol{\theta}) \Big] d\Omega + \lambda \int_\Omega \frac{1}{2} (\boldsymbol{\mathscr{D}}_n \boldsymbol{u})^T\ \widetilde{\boldsymbol{N}}\, \boldsymbol{\mathscr{D}}_n \boldsymbol{u} d\Omega \tag{1}$$

where $\boldsymbol{u} = \{u_1\ \ u_2\ \ u_3\}^T$ is the translational displacements vector of the reference surface points, $\boldsymbol{\theta} = \{\theta_1\ \ \theta_2\}^T$ is the vector containing the rotations of the transverse sections and the operators $\boldsymbol{\mathscr{D}}_p$, $\boldsymbol{\mathscr{D}}_n$ and $\boldsymbol{\mathscr{L}}$ are defined as

$$\boldsymbol{\mathscr{D}}_p = \begin{bmatrix} \dfrac{\partial}{\partial x_1} & 0 & 0 \\ 0 & \dfrac{\partial}{\partial x_2} & 0 \\ \dfrac{\partial}{\partial x_2} & \dfrac{\partial}{\partial x_1} & 0 \end{bmatrix}, \qquad \boldsymbol{\mathscr{D}}_n = \begin{bmatrix} 0 & 0 & \dfrac{\partial}{\partial x_1} \\ 0 & 0 & \dfrac{\partial}{\partial x_2} \\ 0 & 0 & 0 \end{bmatrix} \qquad \boldsymbol{\mathscr{L}} = \begin{bmatrix} 1 & 0 \\ 0 & 1 \\ 0 & 0 \end{bmatrix} \tag{2}$$

In Eq. (1), λ is a load multiplier applied to the pre-buckling membrane forces per unit length $\widetilde{N}_{ij}$ arranged in the matrix $\widetilde{\boldsymbol{N}}$ as follows

$$\widetilde{\boldsymbol{N}} = \begin{bmatrix} \widetilde{N}_{11} & \widetilde{N}_{12} & 0 \\ \widetilde{N}_{12} & \widetilde{N}_{22} & 0 \\ 0 & 0 & 0 \end{bmatrix} \tag{3}$$

Also, $\boldsymbol{A}$, $\boldsymbol{B}$, $\boldsymbol{D}$ and $\boldsymbol{S}$ are the plate extensional, bending–extensional, bending and shear stiffness matrices, respectively, whose definition is given in Appendix A. Note, the stiffness matrices and the pre-buckling membrane forces per unit length are in general function of the position, namely of the x_1 and x_2 coordinates, due to the material and fibre angle distribution and the crack presence.

2.1. Ritz solution

The Ritz solution is based on the approximate representation of the unknown fields in terms of a finite series expansion of known trial functions satisfying the essential boundary condition weighted

by unknown coefficients [63]. For the problem at hand this writes as

$$\begin{Bmatrix} u_1 \\ u_2 \\ u_3 \\ \theta_1 \\ \theta_2 \end{Bmatrix} = \left[\begin{array}{ccc:cc} \boldsymbol{\Psi}_u & \mathbf{0} & \mathbf{0} & \mathbf{0} & \mathbf{0} \\ \mathbf{0} & \boldsymbol{\Psi}_v & \mathbf{0} & \mathbf{0} & \mathbf{0} \\ \mathbf{0} & \mathbf{0} & \boldsymbol{\Psi}_w & \mathbf{0} & \mathbf{0} \\ \hdashline \mathbf{0} & \mathbf{0} & \mathbf{0} & \boldsymbol{\Psi}_{\theta_1} & \mathbf{0} \\ \mathbf{0} & \mathbf{0} & \mathbf{0} & \mathbf{0} & \boldsymbol{\Psi}_{\theta_2} \end{array}\right] \begin{Bmatrix} \boldsymbol{X}_u \\ \boldsymbol{X}_v \\ \boldsymbol{X}_w \\ \boldsymbol{X}_{\theta_1} \\ \boldsymbol{X}_{\theta_2} \end{Bmatrix} = \left[\begin{array}{c:c} \boldsymbol{\Phi_u} & \mathbf{0} \\ \hdashline \mathbf{0} & \boldsymbol{\Phi_\theta} \end{array}\right] \boldsymbol{X} = \boldsymbol{\Phi} \boldsymbol{X} \tag{4}$$

where $\boldsymbol{\Psi}_\chi$, $\chi \in \{u_1, u_2, u_3, \theta_1, \theta_2\}$, is a row matrix collecting the trial functions used for the variable χ and $\boldsymbol{X}_\chi$ is the column vector collecting the corresponding unknown Ritz coefficients;

Substituting Eq. (4) into Eq. (1) and invoking the stationarity condition with respect to the unknowns $\boldsymbol{X}$, the discrete governing equations for the buckling problem are obtained as

$$\left(\boldsymbol{K} + \lambda \boldsymbol{K}_G\right) \boldsymbol{X} = \mathbf{0} \tag{5}$$

which configures a linear eigenvalue problem, being the eigenvalue λ the buckling load multiplier and $\boldsymbol{X}$ the associated eigenvector describing the buckling mode. The matrices involved in Eq. (5) are defined as (see Refs. [62, 60] for more details on their derivation)

$$\boldsymbol{K} = \int_\Omega \begin{bmatrix} \mathcal{B}_{pu}^T \boldsymbol{A} \mathcal{B}_{pu} + \mathcal{B}_{nu}^T \boldsymbol{S} \mathcal{B}_{nu} & \mathcal{B}_{pu}^T \boldsymbol{B} \mathcal{B}_{p\theta} + \mathcal{B}_{nu}^T \boldsymbol{S} \mathcal{B}_{i\theta} \\ \mathcal{B}_{p\theta}^T \boldsymbol{B} \mathcal{B}_{pu} + \mathcal{B}_{i\theta}^T \boldsymbol{S} \mathcal{B}_{nu} & \mathcal{B}_{p\theta}^T \boldsymbol{D} \mathcal{B}_{p\theta} + \mathcal{B}_{i\theta}^T \boldsymbol{S} \mathcal{B}_{i\theta} \end{bmatrix} d\Omega \tag{6a}$$

$$\boldsymbol{K}_G = \int_\Omega \begin{bmatrix} \mathcal{B}_n^T \widetilde{\boldsymbol{N}} \mathcal{B}_{nu} & \mathbf{0} \\ \mathbf{0} & \mathbf{0} \end{bmatrix} d\Omega \tag{6b}$$

where the discrete strain operators are given by

$$\mathcal{B}_{pu} = \mathscr{D}_p \boldsymbol{\Phi_u} \tag{7a}$$

$$\mathcal{B}_{p\theta} = \mathscr{D}_p \mathscr{L} \boldsymbol{\Phi_\theta} \tag{7b}$$

$$\mathcal{B}_{nu} = \mathscr{D}_n \boldsymbol{\Phi_u} \tag{7c}$$

$$\mathcal{B}_{i\theta} = \mathscr{L} \boldsymbol{\Phi_\theta} \tag{7d}$$

2.2. X-Ritz generalized displacement approximation

In the proposed Ritz approach, the admissible functions employed to approximate the plate generalized displacements $\chi \in \{u_1,\, u_2,\, u_3,\ \theta_1,\, \theta_2\}$ are composed of two part. The first, denoted by χ_b and referred as *basic trial functions*, satisfies the geometric and boundary condition of the plate without crack; the second, denoted by χ_c and referred as *crack trial functions*, accounts for the crack discontinuity and singular behaviour. Thus one writes

$$\chi = \chi_b + \chi_c \tag{8}$$

The basic trial function contribution is expressed in terms of one-dimensional Legendre orthogonal polynomials $\psi_\kappa(\zeta)$ of order κ as

$$\chi_b = f_\chi(\xi,\, \eta) \sum_{m=0}^{M_\chi} \sum_{n=0}^{N_\chi} \psi_m(\xi)\, \psi_n(\eta) C^{(0)}_{\chi_{mn}} \tag{9}$$

where $C^{(0)}_{\chi_{mn}}$ are the unknown Ritz coefficients and f_χ is a suitable function chosen to ensure the fulfillment of the homogeneous essential boundary conditions. It is defined as

$$f_\chi(\xi, \eta) = (1+\xi)^{a_1}(1-\xi)^{a_2}(1+\eta)^{a_3}(1-\eta)^{a_4} \tag{10}$$

where the exponents a_i take the values listed in Table 1 accordingly to the case of constrained or unconstrained edge; note that in Eq.(10) it is assumed that $0^0 = 1$.

	Unconstrained				Constrained			
Edge	a_1	a_2	a_3	a_4	a_1	a_2	a_3	a_4
$\xi = -1$	0	0	0	0	1	0	0	0
$\xi = 1$	0	0	0	0	0	1	0	0
$\eta = -1$	0	0	0	0	0	0	1	0
$\eta = 1$	0	0	0	0	0	0	0	1

Table 1: Possible combination of the exponents in Eq.(10).

It is remarked that the χ_b contribution consists of continuous and regular functions that satisfy the plate kinematical boundary conditions and thus it is able to represent the solution of uncracked plates but unable to describe the crack effects.

The crack trial functions contribution is built using terms able to represent the displacement

jump along the crack as well as the singular behaviour of the crack tips fields. Under the assumption of first order shear deformation theory, for constant stiffness plates, the asymptotic crack tip fields can be assumed behaving as $r^{-\frac{1}{2}}$ when the distance r from the crack tip goes to zero [64–68]. This behaviour can be extended to the case of variable stiffness plate [69–72].

In the present work, for the case of an embedded crack having two crack tips, the crack trial functions are chosen as

$$\begin{aligned}\chi_c = g_\chi(\xi,\,\eta)\Bigg\{ & \sum_{p=1}^{P_\chi^{(11)}}\sum_{q=0}^{p} C_{\chi_{pq}}^{(11)} r_1^{\frac{2p-1}{2}} \cos\frac{2q+1}{2}\phi_1 + \\ & \sum_{p=1}^{P_\chi^{(21)}}\sum_{q=0}^{p} C_{\chi_{pq}}^{(21)} r_2^{\frac{2p-1}{2}} \cos\frac{2q+1}{2}\phi_2 + \\ & r_2^{\alpha_2}\sin^2\frac{\theta_2}{2}\sum_{p=1}^{P_\chi^{(12)}}\sum_{q=0}^{p} C_{\chi_{pq}}^{(12)} r_1^{\frac{2p-1}{2}} \sin\frac{2q+1}{2}\phi_1 + \\ & r_1^{\alpha_1}\sin^2\frac{\theta_1}{2}\sum_{p=1}^{P_\chi^{(22)}}\sum_{q=0}^{p} C_{\chi_{pq}}^{(22)} r_2^{\frac{2p-1}{2}} \sin\frac{2q+1}{2}\phi_2 \Bigg\}\end{aligned} \tag{11}$$

where r_i and ϕ_i are the polar coordinates of the point with coordinates $x(\xi,\eta)$ and $y(\xi,\eta)$ as defined in Fig. 1, the $C_{\chi_{pq}}^{(ij)}$ are the unknown Ritz coefficients and $\alpha_1 = \alpha_2 = 3/2$. The integer values $P_\chi^{(ij)}$ determine the number of terms used in the approximation and might be chosen independently, though they are usually set to a common value. The function g_χ enforces homogeneous essentials boundary conditions on the plate edges and it is defined as

$$g_\chi(\xi,\eta) = (1-\xi^2)(1-\eta^2) \tag{12}$$

Detail on the properties of the functions employed Eq. (11) can be found in Ref. [57].

For edge cracks, to account for the presence of a single tip, the crack trial functions assume a different expression that is obtained from Eq. (11) by setting $P_\chi^{(21)} = P_\chi^{(22)} = 0$, $\alpha_2 = 0$ and $\theta_2 = \pi$; in this case, to allow possible crack opening at the edge, the function g_χ is chosen as in Eq. (10) setting to 0 the exponent associated with the edge intersected by the crack and to 1 all of the others.

The proposed Ritz approximations for the generalised displacements can be compactly expressed

in matricial form as follows

$$\chi = \left\{ \boldsymbol{\Psi}_\chi^{(0)} \quad \boldsymbol{\Psi}_\chi^{(11)} \quad \boldsymbol{\Psi}_\chi^{(12)} \quad \boldsymbol{\Psi}_\chi^{(21)} \quad \boldsymbol{\Psi}_\chi^{(22)} \right\} \begin{Bmatrix} \boldsymbol{C}_\chi^{(0)} \\ \boldsymbol{C}_\chi^{(11)} \\ \boldsymbol{C}_\chi^{(12)} \\ \boldsymbol{C}_\chi^{(21)} \\ \boldsymbol{C}_\chi^{(22)} \end{Bmatrix} = \boldsymbol{\Psi}_\chi \boldsymbol{X}_\chi \tag{13}$$

In Eq. (13) the $1 \times (M_\chi + 1)(N_\chi + 1)$ vector $\boldsymbol{\Psi}_\chi^{(0)}$ contains the basic trial function terms and the $(M_\chi + 1)(N_\chi + 1) \times 1$ vector $\boldsymbol{C}_\chi^{(0)}$ collects the corresponding unknown coefficients; analogously the $1 \times [(P_\chi^{(\alpha\beta)} + 1)(P_\chi^{(\alpha\beta)} + 2) - 2]/2$ vectors $\boldsymbol{\Psi}_\chi^{(\alpha\beta)}$ $(\alpha, \beta = 1, 2)$ collect the crack trial function terms and the $[(P_\chi^{(\alpha\beta)} + 1)(P_\chi^{(\alpha\beta)} + 2) - 2]/2 \times 1$ vectors $\boldsymbol{C}_\chi^{(\alpha\beta)}$ the corresponding coefficients. This way the approximation form presented in Eq. (4) is recast an the resolving system matrices properly defined.

The computation of the integrals involved in the stiffness matrices definition need to be carried out numerically and, considering that integrand functions can exhibit high gradients near the crack tips, appropriate numerical integration schemes need to be implemented for accurate evaluation. Details on applicable integration schemes can be found in Ref. [62].

3. Validation and results

3.1. Validation

As no solution for cracked variable stiffness plates are available in the literature, analyses for classical isotropic and anisotropic plates have been carried out to validate the approach and the implemented computer code.

To this aim, referring to the geometrical sketch of Fig. 2, rectangular plates having edge length $w = 0.24\,m$ and exhibiting different edge aspect ratios b/w, crack length ratios a/w and crack inclinations β have been considered. The plates are loaded in compression by a constant force per unit length N_{22} . They are subjected to different edge boundary conditions defined via the acronym $BC_1BC_2BC_3BC_4$ where for the i-th edge BC_i reads as C, S or F for clamped, simply-supported and free boundary condition, respectively (see Fig. 2).

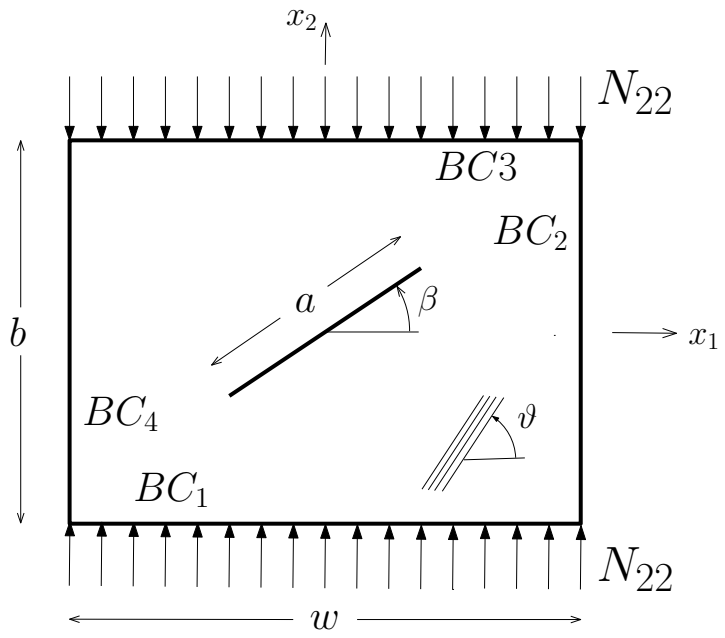

Figure 2: Cracked plate configuration.

Table 2 lists the buckling loads obtained for the case of isotropic isotropic aluminum plates with Young's modulus $E = 70.0\,GPa$, Poisson's coefficient $\nu = 0.3$ and plate thickness $h = 1.2mm$. They have been computed by setting the X-Ritz approximation to $M_\chi = N_\chi = 12$ and $P_\chi^{(11)} = P_\chi^{(12)} = P_\chi^{(21)} = P_\chi^{(22)} = 5$ (see Eqs. (9) and (11)). This approximation scheme provides converged results according to convergence studies not reported here for the sake of conciseness; these convergence studies replicate the method features demonstrated in Ref. [61, 60, 62] for the present variable stiffness implementation.

Table 2: Buckling loads for aluminum plates with edge length $w = 0.24$ [m] and thickness $h = 1.2mmm$

w/b	a/w	Edge BCs	β°	$N_{22}w$	FEM [73]	X-FEM[74]	Exper.[73]
1	0.1	CFCF	0	1782.1	1765.8	1682.3	1627
1	0.3	CFCF	0	1614.0	1602.5	1560.8	1531
1	0.3	CFCF	30	1681.3	1669.7	1630.1	1551
1	0.5	CFCF	60	1703.3	1701.3	1694.9	1636
1	0.5	CFCF	90	1767.6	1765.8	1738.3	1665
1.33	0.3	CFCF	0	1227.4	1217.7	1191.6	1158
2	0.5	CFCF	0	795.5	792.7	754.0	725
1	0.3	SFCF	0	841.7	835.7	833.8	815
1	0.3	SFSF	0	388.9	384.9	406.3	404
1	0.5	SFSF	30	359.6	359.2	390.5	387

An anisotropic, centrally cracked, square plate with $b = w = 0.24\,m$ and thickness $h = 1\,mm$ has been analyzed assuming CFCF edges boundary conditions. The plate consists of a composite lamina with straight fibres layered at an angle ϑ measured with respect to the x_1-axis (see Fig.2). The lamina material properties are given as $E_1 = 206.84\,GPa$, $E_2 = E_3 = 20.684\,GPa$, $G_{13} = 4.1368\,GPa$, $G_{12} = G_{23} = 6.8947\,GPa$, $\nu_{12} = 0.3$ and $\nu_{13} = \nu_{23} = 0.25$. Analyses have been carried out and converged results are presented for the approximation scheme with $M_\chi = N_\chi = 15$ and $P_\chi^{(11)} = P_\chi^{(12)} = P_\chi^{(21)} = P_\chi^{(22)} = 5$. Fig.3 shows the adimensional first buckling load $\bar{N} = \dfrac{12 N_{22} b^2 (1-\nu_{12}^2)}{\pi^2 E_2 h^3}$ for the plate with a central horizontal crack ($\beta = 0^\circ$) of different lengths a/w and various lamina's fibres orientations ϑ. Fig.4 shows the adimensional buckling loads for the first three modes when a central crack with length $a/w = 0.5$ and different inclination β is present in the plate with fibre orientation $\vartheta = 0^\circ$.

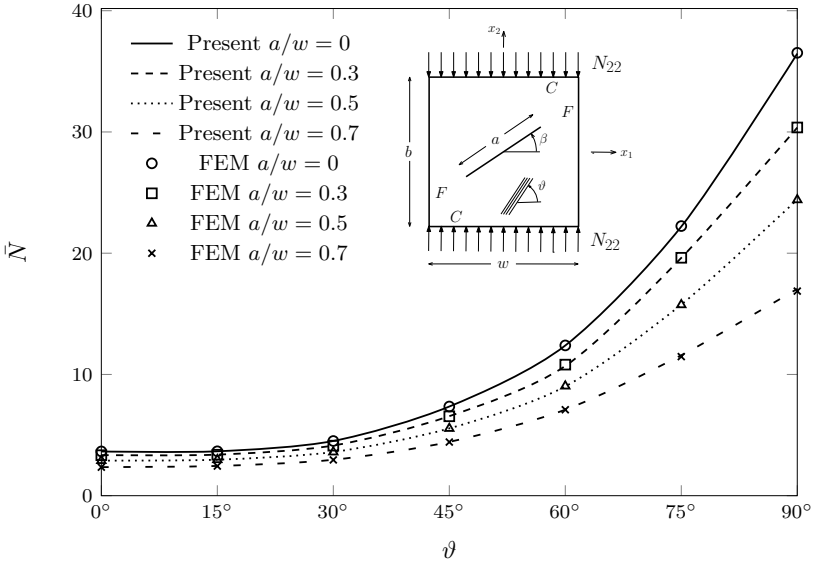

Figure 3: Compression buckling load for the anisotropic CFCF plate with an horizontal crack ($\beta = 0^\circ$) of variable length a/w.

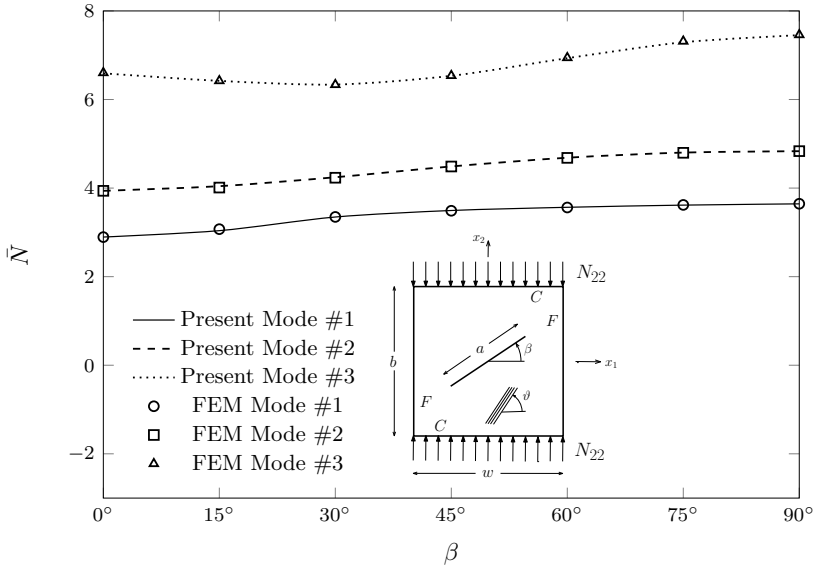

Figure 4: Compression buckling loads (first three modes) for the CFCF plate with fibre angle $\theta = 0^\circ$ and an inclined central crack of length $a/w = 0.5$.

For validation, the present results are checked against those obtained via finite element models solved by Abaqus® . The finite elements results used for comparison have been obtained employing fine mesh models (e.g. 421842 dofs for the $a/w = 0.5$ and $\beta = 45^\circ$ crack case) verified for both displacement and stress resultants accuracy by carrying out convergence studies; this standard convergence studies are not reported here for the sake of coinciseness.The comparison between the present and finite element results shows a very good agreement demonstrating the accuracy and potentiality of the proposed approach. The results obtained for this plate configuration show that the relative angle between the crack orientation and the applied load direction influence the buckling load (see Fig.4). This is due to a redistribution of the pre-buckling stresses caused by the presence of the crack. Furthermore, being the stress components strongly affected by the fiber direction, a value of the relative angle between the crack direction and the fiber direction greater than 15° significantly influence the plate stability. This effect is even more pronounced for longer cracks (see Fig.3).

3.2. Cracked VAT lamina

Let us consider a square plate with $b = w = 0.24\,m$ thickness $h = 1\,mm$. The plate has variable stiffness obtained by using a fiber-reinforced composite with fibres laid at a variable angle ϑ (see Fig.

5a). Referring to Fig.5b, the angle ϑ varies according to the following law holding along the baseline $\mathbf{r}$

$$\vartheta = \vartheta_0 + \frac{\vartheta_A r_B - \vartheta_B r_A}{r_B - r_A} + |r| \frac{\vartheta_B - \vartheta_A}{r_B - r_A} \tag{14}$$

where ϑ_0 is the inclination of the the baseline with respect to the x_1 axis, ϑ_A and ϑ_B are the fibre angles with respect to the baseline at the distances r_A and r_B from the projection O' of the plate center on the baseline (see Fig.5b). According to Gurdal [25], assuming that the point A corresponds to the origin of r, namely $r_A = 0$, and fixing $r_B - r_A = r_B = d$, such a fiber path can be briefly indicated as $\vartheta_0 + \langle \vartheta_A | \vartheta_B \rangle$.

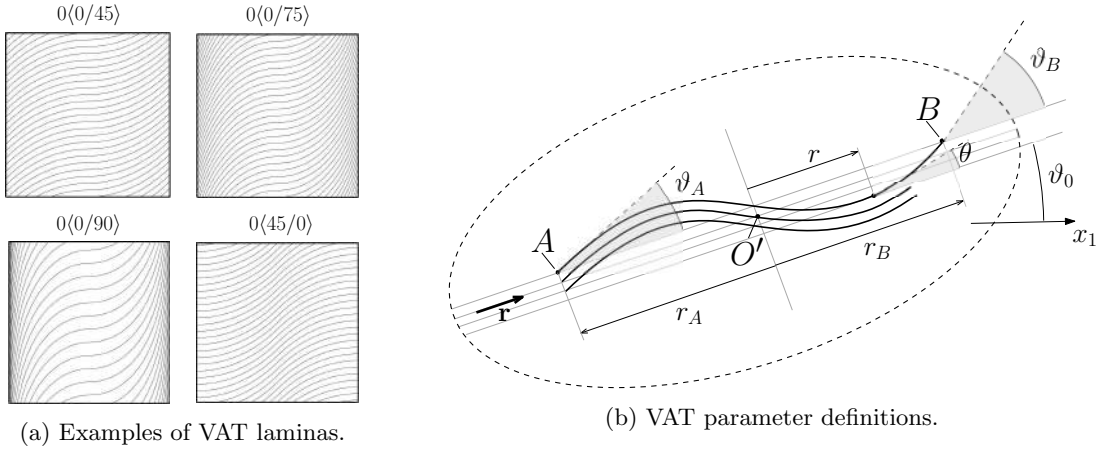

(a) Examples of VAT laminas.

(b) VAT parameter definitions.

Figure 5: VAT laminas examples and VAT parameters definitions.

Buckling analyses have been carried out for cracked plates loaded in compression by a constant force per unit length N_{22} (see Fig. 2). Assuming $\mathbf{r}$ parallel to the x_1 axis, $r_A = 0$ and $r_B = d = w/2$, plates with lamination $0 + \langle \vartheta_A | \vartheta_B \rangle$ and different boundary conditions have been analysed considering the presence of a crack at the plate centre. The material properties are given as $E_1 = 206.84\,GPa$, $E_2 = E_3 = 20.684\,GPa$, $G_{13} = 4.1368\,GPa$, $G_{12} = G_{23} = 6.8947\,GPa$, $\nu_{12} = 0.3$ and $\nu_{13} = \nu_{23} = 0.25$. Regarding to the selected plate's configurations, it is worth nothing that VAT composites allow for a very wide range of possible lamina configurations. Therefore, parametric studies about their behaviour are difficult to present in a comprehensive and clear form; in this sense restricting the investigation to $0 + \langle \vartheta_A | \vartheta_B \rangle$ plates aims to show the potentiality of the proposed approach and to evidence the peculiarity and versatility of variable stiffness composites for plate's structural design. Figs 6, 7, 8 and 9 report the adimensional buckling load $\bar{N} = \dfrac{12 N_{22} b^2 (1 - \nu_{12}^2)}{\pi^2 E_2 h^3}$ of plates with CFCF, CSCS, SSSS and CCCC

boundary conditions, respectively, as function of the ϑ_B parameter for different values of ϑ_A, different crack lengths a/w and crack's inclination β. For comparison purposes, the plots also report with a circle mark the buckling loads for the case of straight fibres as obtained by finite elements in Abaqus®. The data evidence that the crack presence strongly influences the pre-buckling stress distribution and, depending on the kind of assumed boundary conditions, its presence can determine reductions or increments in the buckling loads. This influence is less or more pronounced depending on the crack length and inclination. In particular, results shows that cracks with a length $a > 0.5w$ strongly influence both the buckling load and the buckling mode, triggering a shift of the first buckling mode towards higher modes or more complex buckled configuration. On the other hand, smaller cracks shows to have more influence on the buckling load only, with an effect that vary with fiber path and crack inclination. Note that some configurations, generally associated with long horizontal cracks, also admit traction buckling loads as a consequence of complex pre-buckling stress distributions (see Figs 7d, 7g, 8d, 8g, 9a, 9d, 9g). From the damage tolerant design point of view, this circumstance should be adequately addressed in the design. However, the most meaningful feature illustrated by the presented results consists in the variability of the buckling load with respect to the fibre paths for a given crack configuration. As expected, the buckling behaviour of the center-cracked VAT plates is strongly influenced by the value of the fiber angle at the plate center, thus confirming that the value of the relative angle between the crack direction and the fiber direction plays and important role for the plate stability. This means that an appropriate selection of the fibre path can afford a redistribution of the pre-buckling stresses within the plate providing a desired level of buckling load (within a suitable range) even in presence of a crack, opening to interesting possibility in the framework of damage tolerant design approach. To complete the picture, Figs 10, 11, 12 and 13 show the buckling mode for analysed plates with with CFCF, CSCS, SSSS and CCCC boundary conditions, respectively. Note both the buckling mode shape variation with respect to the fibre path and the different modal shapes between compression and traction buckling.

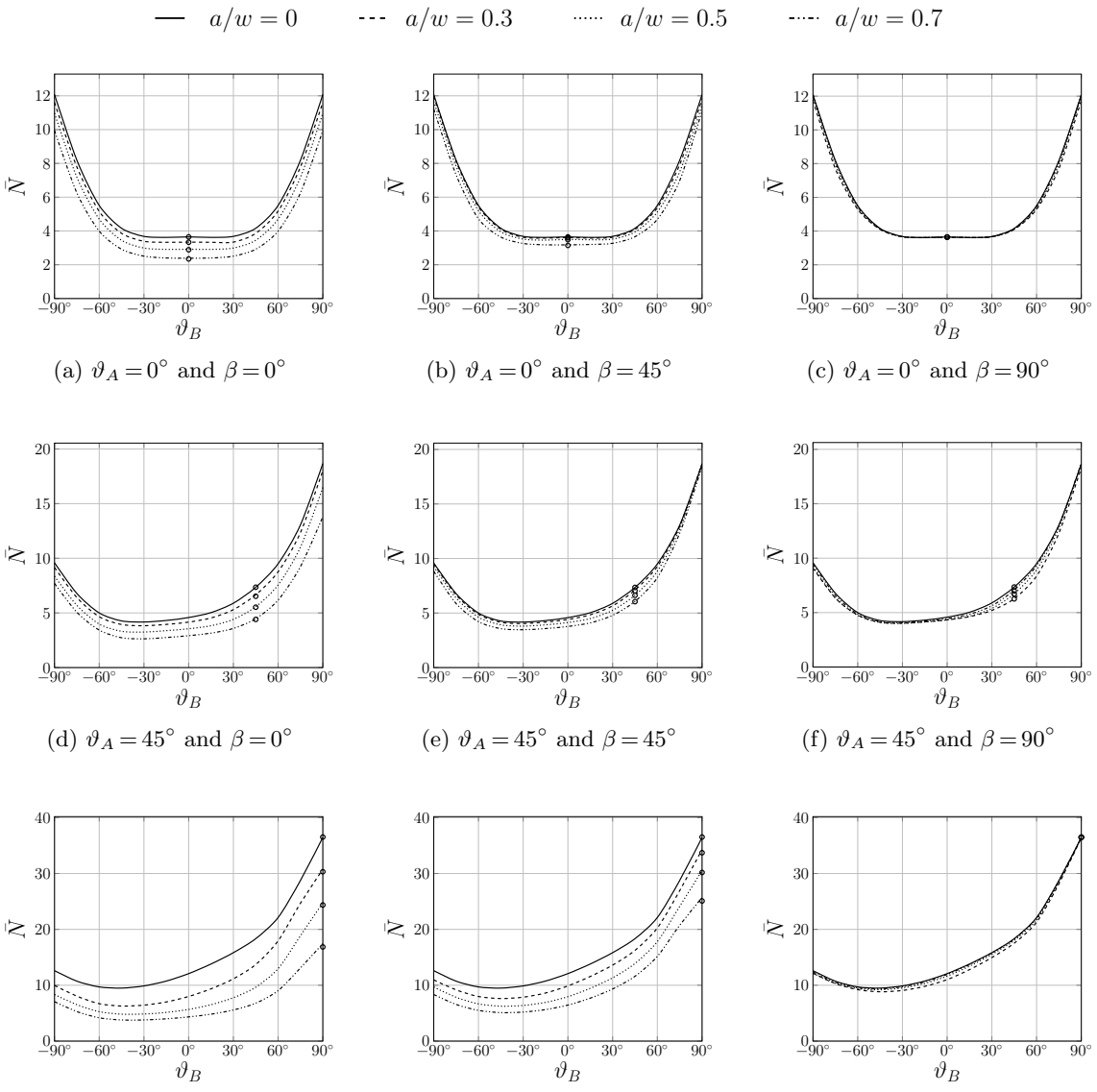

(a) $\vartheta_A = 0^\circ$ and $\beta = 0^\circ$ (b) $\vartheta_A = 0^\circ$ and $\beta = 45^\circ$ (c) $\vartheta_A = 0^\circ$ and $\beta = 90^\circ$

(d) $\vartheta_A = 45^\circ$ and $\beta = 0^\circ$ (e) $\vartheta_A = 45^\circ$ and $\beta = 45^\circ$ (f) $\vartheta_A = 45^\circ$ and $\beta = 90^\circ$

(g) $\vartheta_A = 90^\circ$ and $\beta = 0^\circ$ (h) $\vartheta_A = 90^\circ$ and $\beta = 45^\circ$ (i) $\vartheta_A = 90^\circ$ and $\beta = 90^\circ$

Figure 6: Buckling loads for the center-cracked CFCF square VAT plate loaded in compression

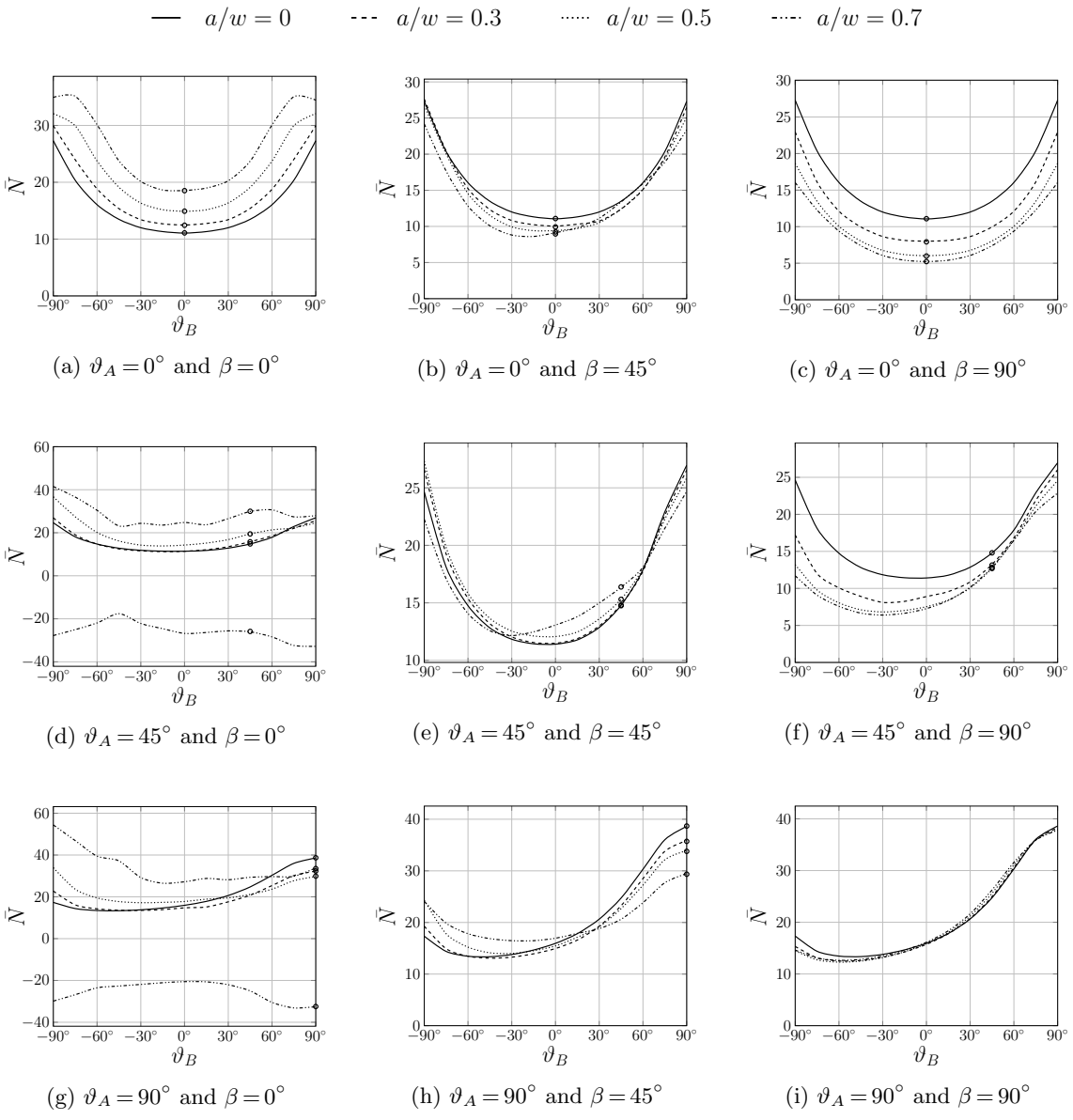

(a) $\vartheta_A = 0^\circ$ and $\beta = 0^\circ$ (b) $\vartheta_A = 0^\circ$ and $\beta = 45^\circ$ (c) $\vartheta_A = 0^\circ$ and $\beta = 90^\circ$

(d) $\vartheta_A = 45^\circ$ and $\beta = 0^\circ$ (e) $\vartheta_A = 45^\circ$ and $\beta = 45^\circ$ (f) $\vartheta_A = 45^\circ$ and $\beta = 90^\circ$

(g) $\vartheta_A = 90^\circ$ and $\beta = 0^\circ$ (h) $\vartheta_A = 90^\circ$ and $\beta = 45^\circ$ (i) $\vartheta_A = 90^\circ$ and $\beta = 90^\circ$

Figure 7: Buckling loads for the center-cracked CSCS square VAT plate loaded in compression

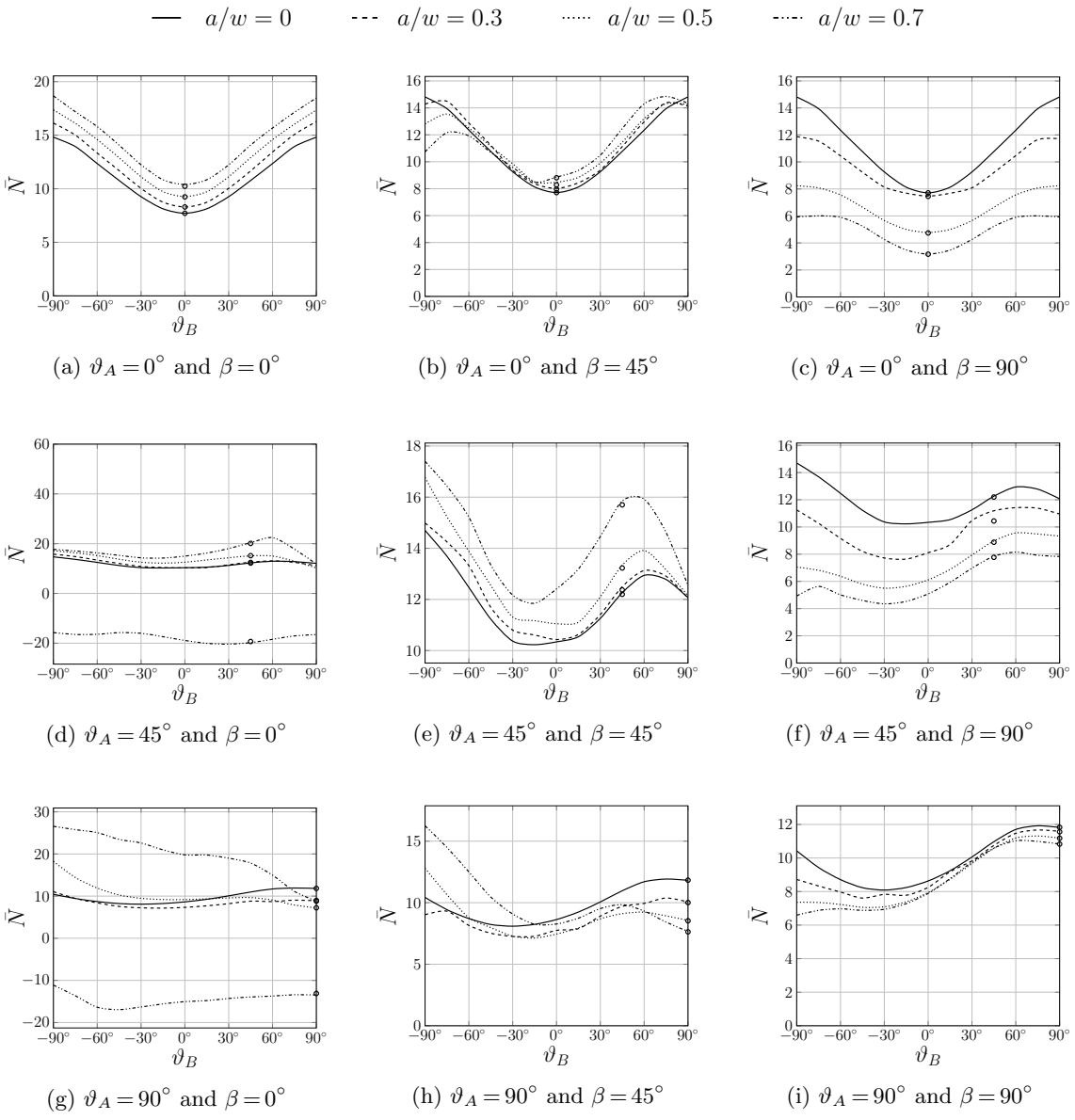

(a) $\vartheta_A = 0^\circ$ and $\beta = 0^\circ$ (b) $\vartheta_A = 0^\circ$ and $\beta = 45^\circ$ (c) $\vartheta_A = 0^\circ$ and $\beta = 90^\circ$

(d) $\vartheta_A = 45^\circ$ and $\beta = 0^\circ$ (e) $\vartheta_A = 45^\circ$ and $\beta = 45^\circ$ (f) $\vartheta_A = 45^\circ$ and $\beta = 90^\circ$

(g) $\vartheta_A = 90^\circ$ and $\beta = 0^\circ$ (h) $\vartheta_A = 90^\circ$ and $\beta = 45^\circ$ (i) $\vartheta_A = 90^\circ$ and $\beta = 90^\circ$

Figure 8: Buckling loads for the center-cracked SSSS square VAT plate loaded in compression

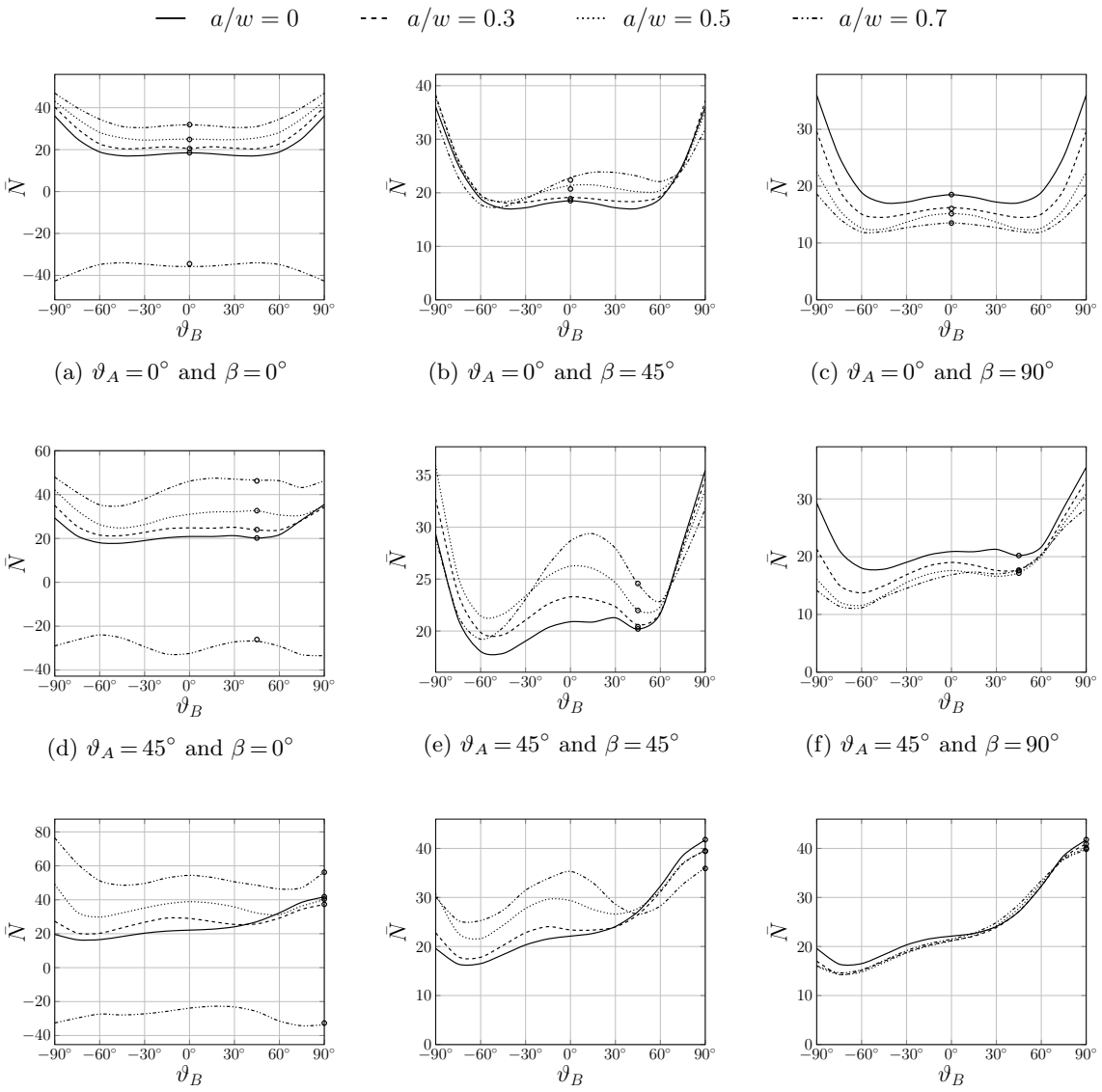

(a) $\vartheta_A = 0^\circ$ and $\beta = 0^\circ$ (b) $\vartheta_A = 0^\circ$ and $\beta = 45^\circ$ (c) $\vartheta_A = 0^\circ$ and $\beta = 90^\circ$

(d) $\vartheta_A = 45^\circ$ and $\beta = 0^\circ$ (e) $\vartheta_A = 45^\circ$ and $\beta = 45^\circ$ (f) $\vartheta_A = 45^\circ$ and $\beta = 90^\circ$

(g) $\vartheta_A = 90^\circ$ and $\beta = 0^\circ$ (h) $\vartheta_A = 90^\circ$ and $\beta = 45^\circ$ (i) $\vartheta_A = 90^\circ$ and $\beta = 90^\circ$

Figure 9: Buckling loads for the center-cracked CCCC square VAT plate loaded in compression

$(\vartheta_A,\, \vartheta_B)$	$a/w = 0.0$	$a/w = 0.3$	$a/w = 0.5$	$a/w = 0.7$
$(90°,\, -90°)$	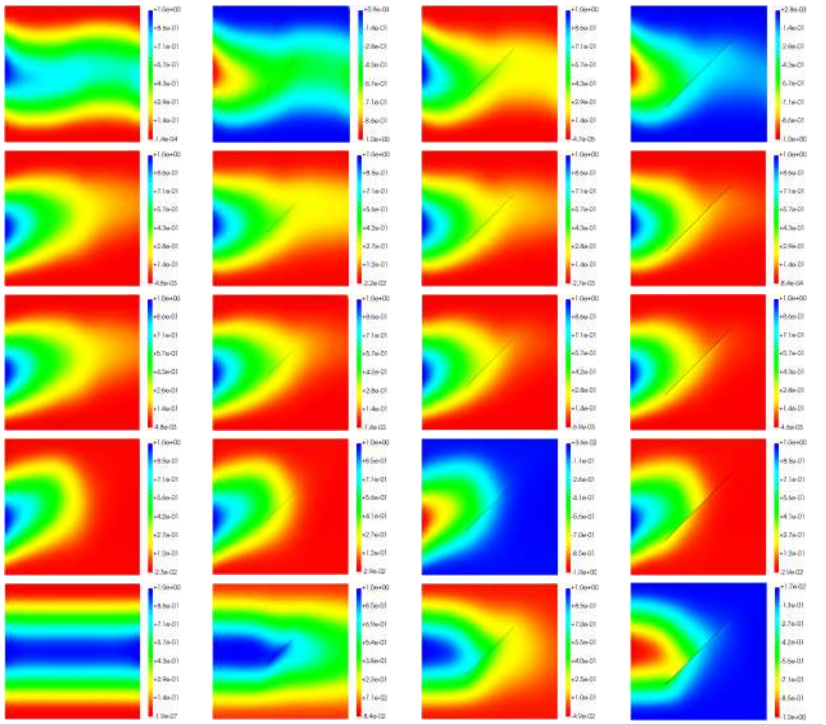			
$(90°,\, -45°)$				
$(90°,\, 0°)$				
$(90°,\, 45°)$				
$(90°,\, 90°)$				

Figure 10: CFCF VAT lamina buckling first mode with a 45° inclined crack

$(\vartheta_A,\ \vartheta_B)$	$a/w = 0.0$	$a/w = 0.3$	$a/w = 0.5$	$a/w = 0.7$ compr.	$a/w = 0.7$ trac.
$(45°,\ -90°)$	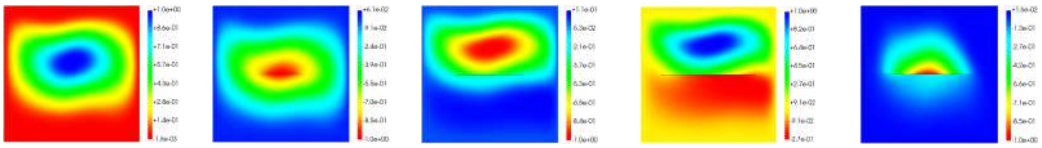				
$(45°,\ -45°)$	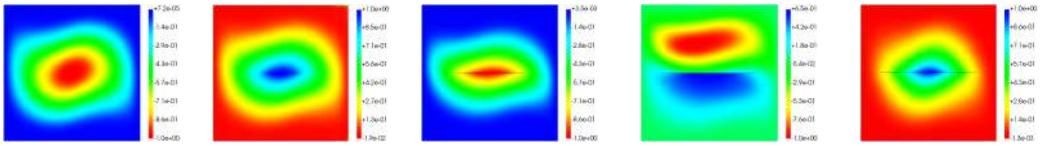				
$(45°,\ 0°)$	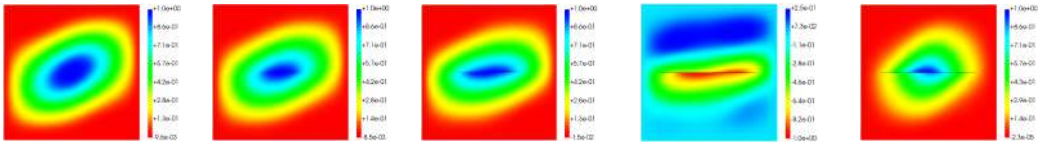				
$(45°,\ 45°)$	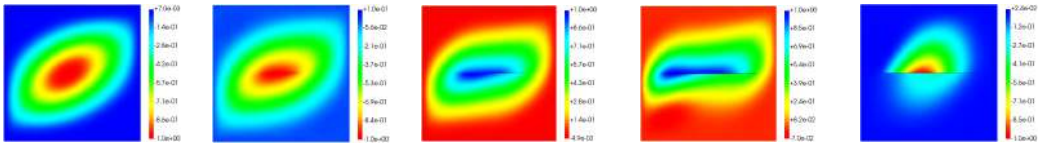				
$(45°,\ 90°)$	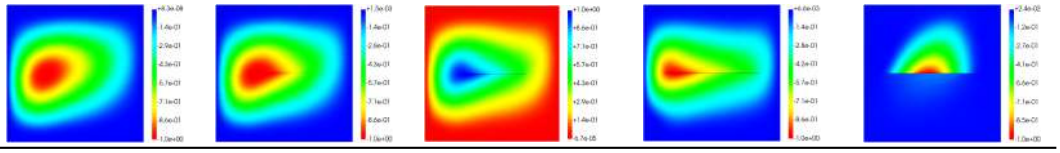				

Figure 11: CSCS VAT lamina buckling first mode horizontal crack

$(\vartheta_A,\, \vartheta_B)$	$a/w = 0.0$	$a/w = 0.3$	$a/w = 0.5$	$a/w = 0.7$
$(45°,\, -90°)$	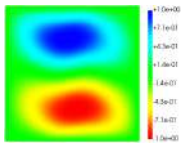	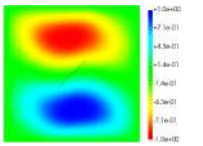	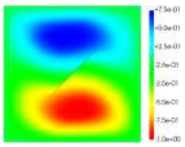	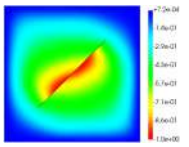
$(45°,\, -45°)$	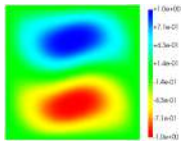	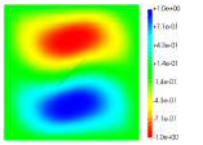	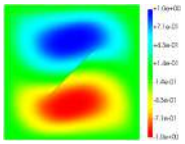	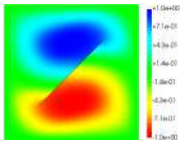
$(45°,\, 0°)$	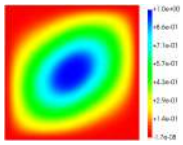	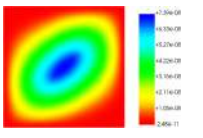	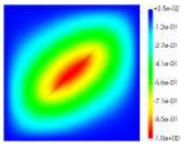	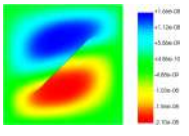
$(45°,\, 45°)$	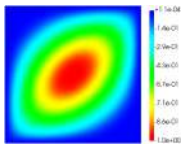	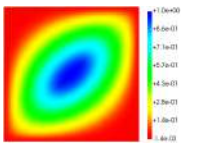	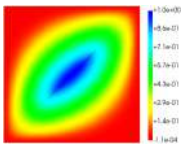	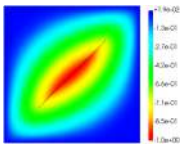
$(45°,\, 90°)$	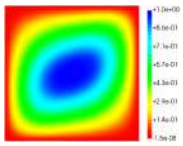	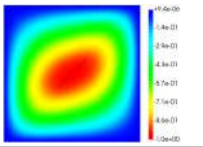	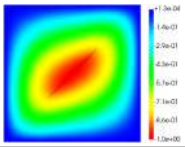	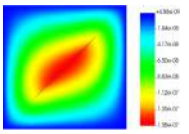

Figure 12: SSSS VAT lamina compression buckling first mode 45 inclined crack

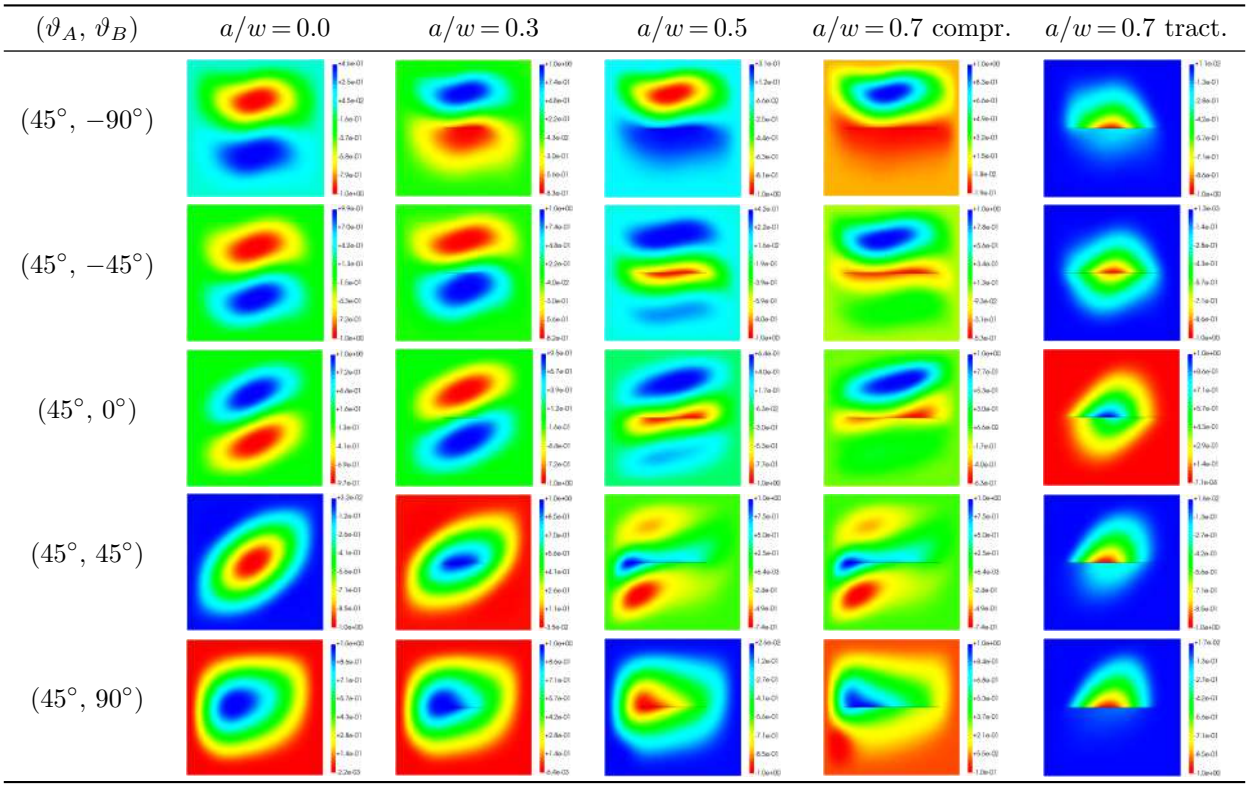

Figure 13: CCCC VAT lamina compression buckling first mode 0 inclined crack

3.3. VAT laminates

As observed in the preceding section, a rigorous and comprehensive parametric study of buckling for variable stiffness composite cracked, one layer plates is not feasible due to the huge number of possible different configurations with a change of the involved parameters. This is even more evident for VAT laminates where the stacking sequence plays the role of a massive multiplier of achievable configurations. Thus, in the present paper, to investigate the effects of cracks on the buckling behaviour of VAT laminates, the analyzed configurations are restricted to those proposed in Ref [25], which are considered sufficiently representative to illustrate features and potentialities of VAT laminates. These consists of twelve layers $[0 \pm \langle \vartheta_A/\vartheta_B \rangle]_{3S}$ and $[90 \pm \langle \vartheta_A/\vartheta_B \rangle]_{3S}$ square laminated plates undergoing to uniform end shortening u_0 along the x_1 axis. The plates are simply-supported with the transverse edge restrained in the direction orthogonal to the applied end shortening for the $[0 \pm \langle \vartheta_A/\vartheta_B \rangle]_{3S}$ laminate and free to deform for the $[90 \pm \langle \vartheta_A/\vartheta_B \rangle]_{3S}$ case, respectively. The material properties are assumed as $E_1 = 181.0\,GPa$, $E_2 = 10.3\,GPa$, $G_{31} = 7.0\,GPa$, $G_{32} = 3.0\,GPa$, $G_{12} = 7.17\,GPa$, $\nu_{12} = 0.28$ and the

ply thickness is $0.127\,mm$ corresponding to a laminate thickness $h = 1.524\,mm$. Note, non uniform distributions of stresses generally arise in the pre-buckling state of variable stiffness laminates, which suggests the introduction of an average critical buckling load N_{cr}^{av} and a plate overall axial stiffness E_1^{eq} defined as [25]

$$N_{cr}^{av} = \frac{1}{b}\int_{-b/2}^{b/2} N_{11}\left(w/2, x_2\right) dx_2 \tag{15a}$$

$$E_1^{eq} = \frac{w\int_{-b/2}^{b/2} N_{11}\left(w/2, x_2\right) dx_2}{2\ h\ b\ u_0} \tag{15b}$$

where the involved quantities are defined with reference to the geometrical scheme of Fig.1. It is worth to mention that both N_{cr}^{av} and E_1^{eq} depend on the values of ϑ_A and ϑ_B; their adimensional counterparts $\dfrac{N_{cr}^{av} w^2}{E_1 h^3}$ and E_1^{eq}/E_1, respectively, are used to present and discuss the results obtained for the buckling of VAT laminates. These have been obtained considering an approximation scheme with $M_\chi = N_\chi = 24$ and $P_\chi^{(11)} = P_\chi^{(12)} = P_\chi^{(21)} = P_\chi^{(22)} = 5$ (see Eqs. (9) and (11)), which was proven to provide converged result.

Figs. 14 and 15 show the buckling results for the $[0\pm\langle\vartheta_A/\vartheta_B\rangle]_{3S}$ and $[90\pm\langle\vartheta_A/\vartheta_B\rangle]_{3S}$ undamaged plates, respectively. The present results can be considered in good agreement with those reported in Ref. [25] where the classical lamination theory (CLT) is employed, being the differences related to the use of the first order shear theory (FSDT) in the present approach. This circumstance is depicted in Fig 16 where representative results from the present approach in the framework of CLT, obtained by penalizing the shear energy terms, are also presented.

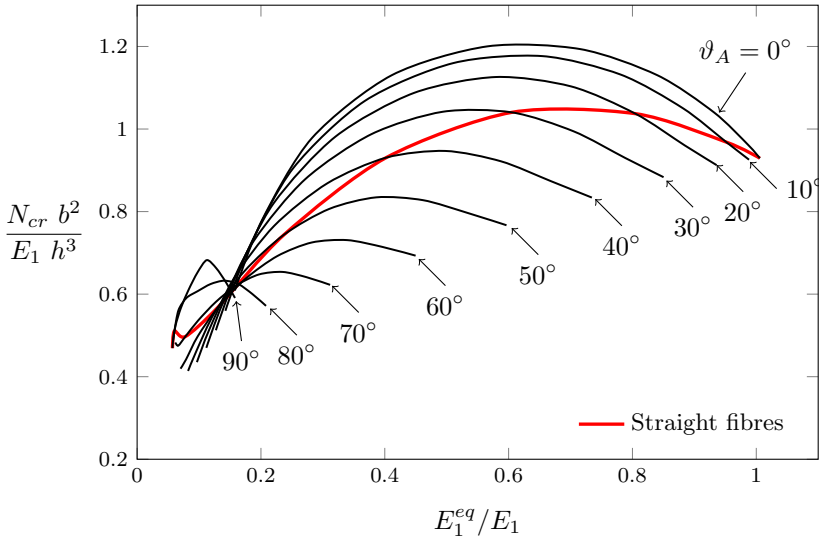

Figure 14: Buckling of the simply-supported, square VAT $[0 \pm \langle \vartheta_A/\vartheta_B \rangle]_{3S}$ laminate without crack under uniform end shortening along x_1.

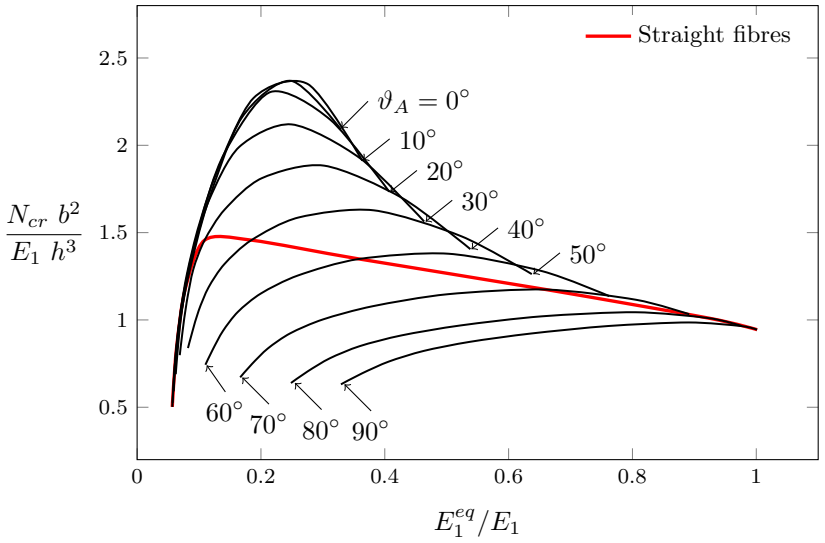

Figure 15: Buckling of the simply-supported, square VAT $[90 \pm \langle \vartheta_A/\vartheta_B \rangle]_{3S}$ laminate without crack under uniform end shortening along x_1.

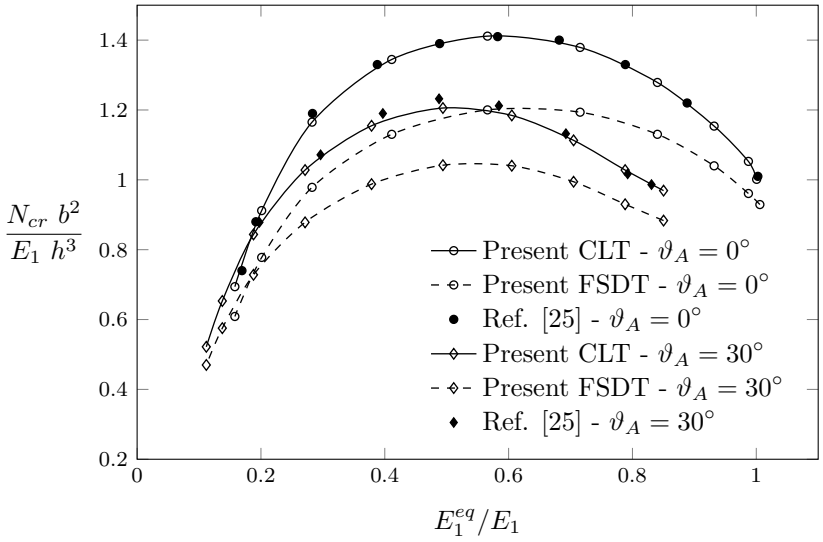

Figure 16: Buckling of the simply-supported, square VAT $[0 \pm \langle \vartheta_A/\vartheta_B \rangle]_{3S}$ laminate without crack under uniform end shortening along x_1: comparison of different plate theories

In the framework of the first order shear deformation theory, as expected, the present results confirm previous findings about the option to improve the buckling performances of uncracked laminates by selecting suitable fiber paths. Figs. 17, 18 and 19 show the buckling results for the $[0 \pm \langle \vartheta_A/\vartheta_B \rangle]_{3S}$ laminate configuration when an horizontal ($\beta = 0°$), inclined ($\beta = 45°$) and vertical ($\beta = 90°$) crack of length $a/w = 0.5$ is present, respectively. Analogously, Figs. 20, 21 and 22 show the same kind of results for the $[90 \pm \langle \vartheta_A/\vartheta_B \rangle]_{3S}$ laminate.

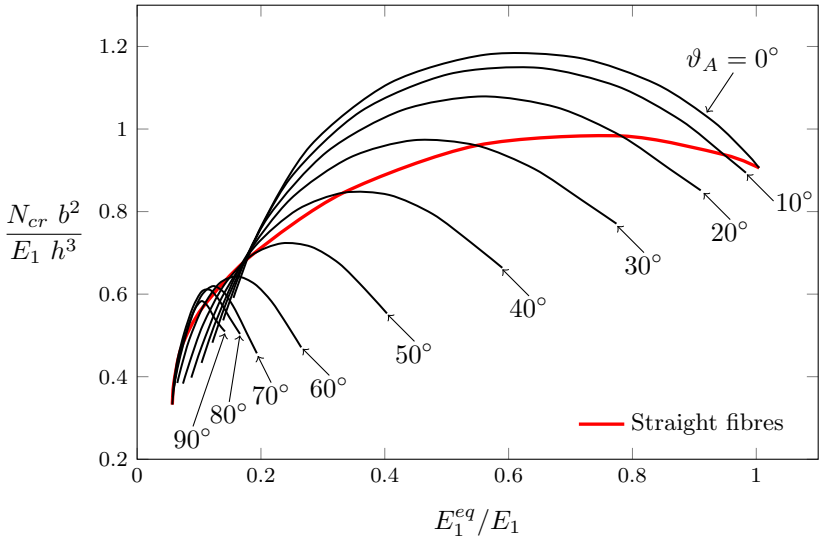

Figure 17: Buckling of the simply-supported, square VAT $[0 \pm \langle \theta_A/\vartheta_B \rangle]_{3S}$ laminate with a $a/w = 0.5$ horizontal ($\beta = 0°$) crack under uniform end shortening along x_1.

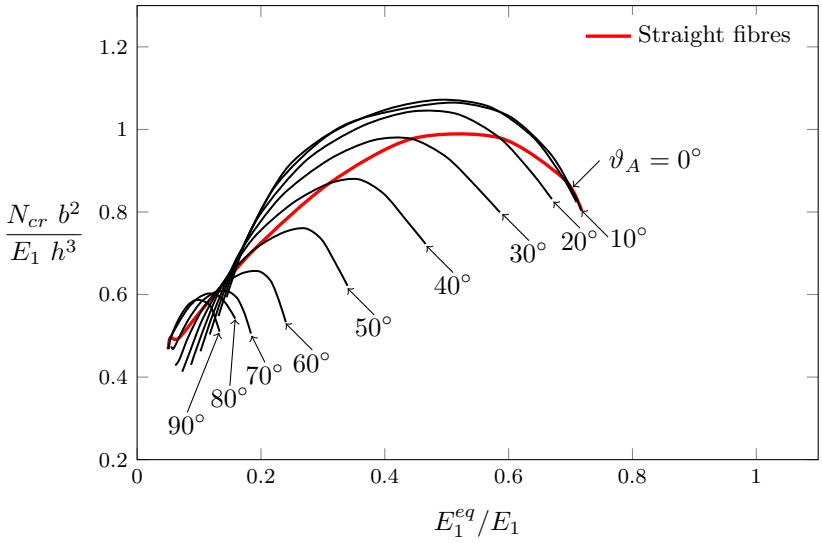

Figure 18: Buckling of the simply-supported, square VAT $[0 \pm \langle \vartheta_A/\vartheta_B \rangle]_{3S}$ laminate with a $a/w = 0.5$ inclined ($\beta = 45°$) crack under uniform end shortening along x_1.

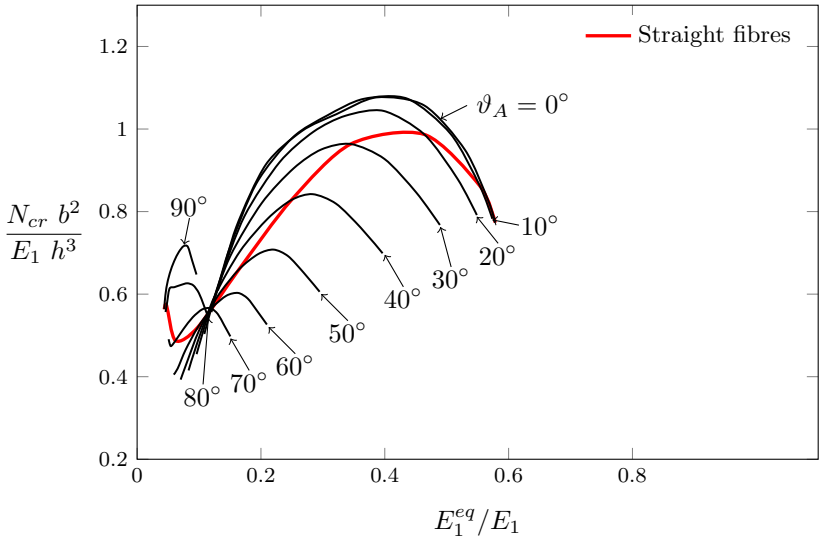

Figure 19: Buckling of the simply-supported, square VAT $[0 \pm \langle \vartheta_A/\vartheta_B \rangle]_{3S}$ laminate with a $a/w = 0.5$ vertical ($\beta = 90°$) crack under uniform end shortening along x_1.

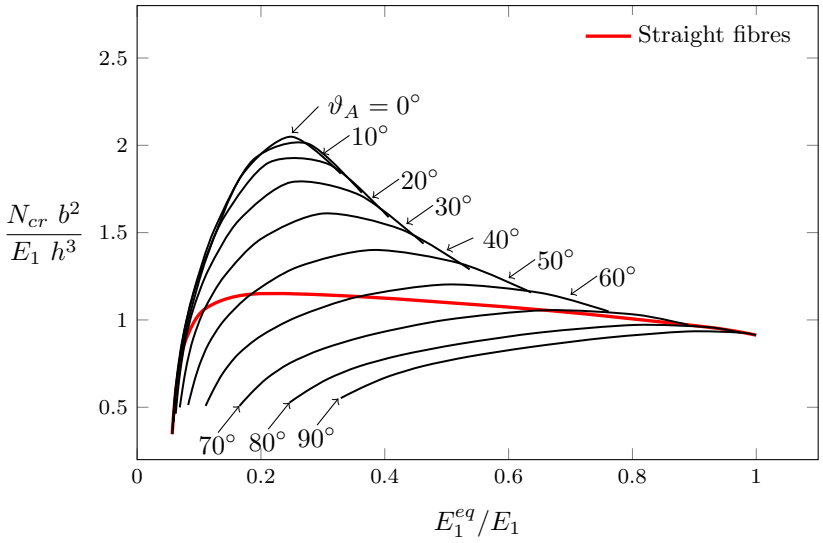

Figure 20: Buckling of the simply-supported, square VAT $[90 \pm \langle \vartheta_A/\vartheta_B \rangle]_{3S}$ laminate with a $a/w = 0.5$ horizontal ($\beta = 0°$) crack under uniform end shortening along x_1.

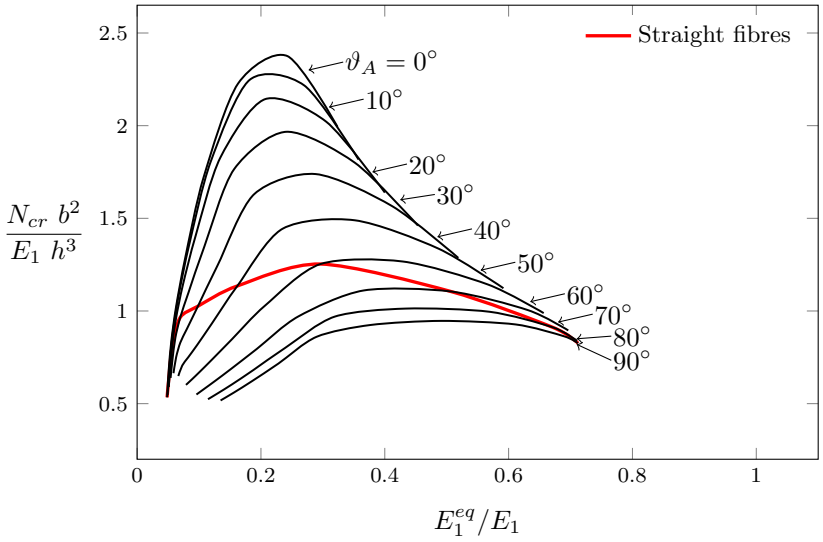

Figure 21: Buckling of the simply-supported, square VAT $[90 \pm \langle \vartheta_A/\vartheta_B \rangle]_{3S}$ laminate with a $a/w = 0.5$ inclined ($\beta = 45°$) crack under uniform end shortening along x_1.

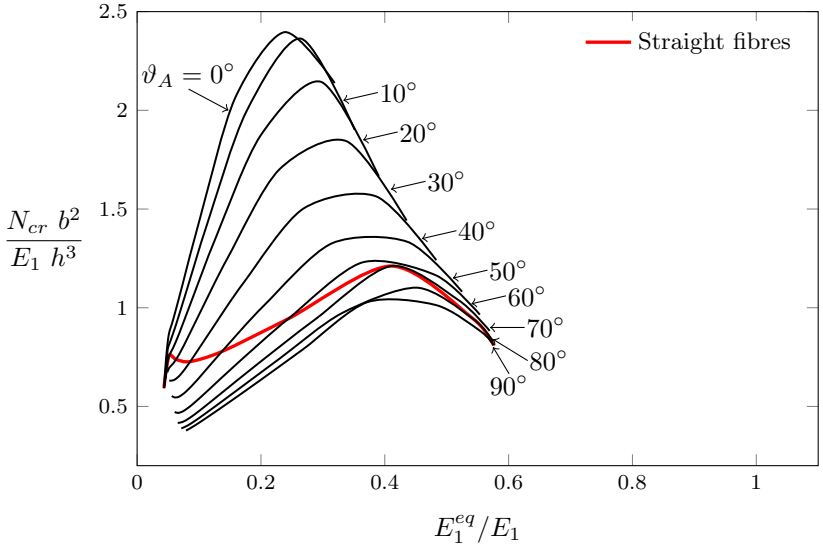

Figure 22: Buckling of the simply-supported, square VAT $[90 \pm \langle \vartheta_A/\vartheta_B \rangle]_{3S}$ laminate with a $a/w = 0.5$ vertical ($\beta = 90°$) crack under uniform end shortening along x_1.

A preliminary analysis of the results shows that both the buckling load and the overall axial stiffness for cracked plates are lower than those of the corresponding uncracked plate. This effect is due to a loss of stiffness along the the direction orthogonal to the crack and, as expected, is more pronounced

for inclined and vertical crack, being the compressive displacement applied along the horizontal direction. The presented results (see Figs 17–22) evidence for both the analyzed configuration the design opportunities offered by the VAT concept also for buckling of cracked laminates; for a laminate with a given crack there are several fibre path able to provide higher buckling loads and higher overall axial stiffness with respect to the straight fibre case. In the framework of damage tolerant approaches, this allows to select fibre paths that, through an appropriate nonuniform pre-buckling stress distribution, allows an improvement of the buckling performance and also guarantee predefined design levels of buckling load and axial stiffness even in presence of cracks.

It is worth to note that the presented results are obtained under the usual equivalent single layer assumptions of constant thickness and perfectly bonded layers, whereas the manufacturing process of VAT can introduce thickness variation and imperfect interfaces (e.g. [75, 76]), both potentially affecting the plate response. Additionally, no constraints have been introduced to avoid interpenetration of the crack faces [47], whose contact can influence the modal shape and buckling loading. In the present work these effects are not considered and their consideration establishes possible future improvements of the approach with the aim of gaining higher fidelity in modeling and more insight in the buckling behaviour of cracked VAT laminates. However, pursuing the aims of this work, the proposed parametric studies allowed to highlight the fundamental features related to the buckling behaviour of cracked VAT composite plates, proving the capabilities of the proposed approach to carry out such a kind of investigations. The developed tool allows different crack position and VAT plate configurations to be efficiently analyzed in order to optimize the plate configuration in a damage tolerant design framework typically required in aeronautical structural certification procedures.

4. Conclusions

In this work, an X-Ritz method for buckling analysis of variable stiffness cracked composite plates has been presented. Within the framework of the first order shear deformation theory, a combination of standard orthogonal polynomials and crack enrichment special functions are used to approximate the problem primary variables. With the benefits of a robust, single-domain meshless method, the proposed approach allows to inherently account for crack tip singular fields and displacement discontinuity, reducing data preparation efforts and required degrees of freedom. Representative case studies for variable angle tow homogeneous and laminated plates, with different crack lengths, inclinations and plate boundary conditions, have been presented and discussed. Although, to the best of the authors'

knowledge, this is the first study proposed in the literature that accounts for crack damages in VAT laminated plates, this work demonstrated the potentiality of the proposed formulation and allowed to highlight the advantages offered by variable angle tow composites for the buckling performances of cracked laminated plates. The work has shown that the presence of the crack alter the plate buckling behaviour depending on the kind of boundary conditions, with an influence that is less or more pronounced depending on the crack length and inclination. Also, this study has shown that some configurations, generally associated with long horizontal cracks, admit traction buckling loads as a consequence of complex pre-buckling stress distributions triggered by the crack presence. Moreover, for variable angle tow laminated plates, the variability of the buckling load with respect to the fibre paths for a given crack configuration suggests that desired levels (within suitable ranges) of plate buckling load and axial overall stiffness can be simultaneously attained by suitably choosing the curvilinear fibre path. These results open to interesting possibilities in the framework of damage tolerant design of variable stiffness laminated structures.

5. Acknowledgments

The first author acknowledge the support of the Italian Ministry of University and Research MUR through the project DEVISU, funded under the scheme PRIN-2107 Grant Nr. 22017ZX9X4K006.

[1] M. Hyer, H. Lee, The use of curvilinear fiber format to improve buckling resistance of composite plates with central circular holes, Composite Structures 18 (1991) 239–261.

[2] Z. Gürdal, R. Olmedo, In-plane response of laminates with spatially varying fiber orientations-variable stiffness concept, AIAA Journal 31 (4) (1993) 751–758.

[3] A. Leissa, A review of laminated composite plate buckling, Applied Mechanics Reviews 40 (5) (1987) 575–591.

[4] C. Chia, Geometrically nonlinear behavior of composite plates: A review, Applied Mechanics Reviews 41 (12) (1988) 439–451.

[5] G. Turvey, I. Marshall (Eds.), Buckling and postbuckling of composite plates, Springer Netherlands, 1995.

[6] A. K. Noor, J. M. Peters, Buckling and postbuckling analyses of laminated anisotropic structures, International Journal for Numerical Methods in Engineering 27 (2) (1989) 383–401.

[7] Y. Kumar, The Rayleigh-Ritz method for linear dynamic, static and buckling behaviour of beams, shells and plates: A literature review, Journal of Vibration and Control (2017) 1077546317694724.

[8] E. Cosentino, P. Weaver, Approximate nonlinear analysis method for debonding of skin/stringer composite assemblies, AIAA Journal 46 (5) (2008) 1144–1159.

[9] C. Mittelstedt, Explicit local buckling analysis of stiffened composite plates accounting for periodic boundary conditions and stiffener-plate interaction, Composite Structures 91 (3) (2009) 249–265.

[10] D. Stamatelos, G. Labeas, K. Tserpes, Analytical calculation of local buckling and post-buckling behavior of isotropic and orthotropic stiffened panels, Thin-Walled Structures 49 (3) (2011) 422–430.

[11] L. Brubak, J. Hellesland, Semi-analytical postbuckling analysis of stiffened imperfect plates with a free or stiffened edge, Computers and Structures 89 (17-18) (2011) 1574–1585.

[12] R. Vescovini, C. Bisagni, Two-step procedure for fast post-buckling analysis of composite stiffened panels, Computers and Structures 128 (2013) 38–47.

[13] H. Zheng, Z. Wei, Vibroacoustic analysis of stiffened plates with nonuniform boundary conditions, International Journal of Applied Mechanics 5 (4).

[14] M. M. Saadatpour, M. Azhari, M. A. Bradford, Analysis of general quadrilateral orthotropic thick plates with arbitrary boundary conditions by the Rayleigh Ritz method, International Journal for Numerical Methods in Engineering 54 (7) (2002) 1087–1102.

[15] R. Rango, F. Bellomo, L. Nallim, A general Ritz algorithm for static analysis of arbitrary laminated composite plates using first order shear deformation theory, Journal of Engineering Research 10 (2) (2013) 1–12.

[16] S. Wang, A unified Timoshenko beam b-spline Rayleigh-Ritz method for vibration and buckling analysis of thick and thin beams and plates, International Journal for Numerical Methods in Engineering 40 (3) (1997) 473–491.

[17] K. Liew, Solving the vibration of thick symmetric laminates by Reissner/Mindlin plate theory and the p-Ritz method, Journal of Sound and Vibration 198 (3) (1996) 343–360.

[18] Y. Cheung, D. Zhou, Vibrations of moderately thick rectangular plates in terms of a set of static Timoshenko beam functions, Computers and Structures 78 (6) (2000) 757–768.

[19] D. Zhou, Vibrations of Mindlin rectangular plates with elastically restrained edges using static Timoshenko beam functions with the Rayleigh-Ritz method, International Journal of Solids and Structures 38 (32-33) (2001) 5565–5580.

[20] S. Eftekhar, A. Jafari, A novel and accurate Ritz formulation for free vibration of rectangular and skew plates, Journal of Applied Mechanics, Transactions ASME 79 (6) (2012) art. no 064504 (5 pages).

[21] S. Eftekhari, A. Jafari, A simple and accurate Ritz formulation for free vibration of thick rectangular and skew plates with general boundary conditions, Acta Mechanica 224 (1) (2013) 193–209.

[22] K. Liew, J. Wang, M. Tan, S.Rajendran, Nonlinear analysis of laminated composite plates using the mesh-free kp-Ritz method based on FSDT, Computer Methods in Applied Mechanics and Engineering 193 (45-47) (2004) 4763–4779.

[23] K. Liew, J. Wang, M. Tan, S. Rajendran, Postbuckling analysis of laminated composite plates using the mesh-free kp-Ritz method, Computer Methods in Applied Mechanics and Engineering 195 (7-8) (2006) 551–570.

[24] Y. Lee, X.Zhao, J. Reddy, Postbuckling analysis of functionally graded plates subject to compressive and thermal loads, Computer Methods in Applied Mechanics and Engineering 199 (25-28) (2010) 1645–1653.

[25] Z. Gürdal, B. Tatting, C. Wu, Variable stiffness composite panels: Effects of stiffness variation on the in-plane and buckling response, Composites Part A: Applied Science and Manufacturing 39 (5) (2008) 911–922.

[26] C. Lopes, Z. Gürdal, P. Camanho, Variable-stiffness composite panels: Buckling and first-ply failure improvements over straight-fibre laminates, Computers and Structures 86 (9) (2008) 897–907.

[27] G. Raju, Z. Wu, B. Kim, P. Weaver, Prebuckling and buckling analysis of variable angle tow plates with general boundary conditions, Composite Structures 94 (9) (2012) 2961–2970.

[28] Z. Wu, P. Weaver, G. Raju, B. Chul Kim, Buckling analysis and optimisation of variable angle tow composite plates, Thin-Walled Structures (163-172) (2012) 60.

[29] Z. Wu, P. Weaver, G. Raju, Postbuckling optimisation of variable angle tow composite plates, Composite Structures 103 (2013) 34–42.

[30] G. Raju, Z. Wu, P. Weaver, Postbuckling analysis of variable angle tow plates using differential quadrature method, Composite Structures 106 (2013) 74–84.

[31] W. Liu, R. Butler, Buckling optimization of variable-angle-tow panels using the infinite-strip method, AIAA Journal 51 (6) (2013) 1442–1449.

[32] Z. Wu, G. Raju, P. Weaver, Postbuckling analysis of variable angle tow composite plates, International Journal of Solids and Structures 50 (10) (2013) 1770–1780.

[33] J. Yang, B. Song, X. Zhong, Parametric study on buckling property of variable angle tow laminates, Fuhe Cailiao Xuebao/Acta Materiae Compositae Sinica 32 (4) (2015) 1145–1152.

[34] G. Raju, Z. Wu, P. Weaver, Buckling and postbuckling of variable angle tow composite plates under in-plane shear loading, International Journal of Solids and Structures 58 (2015) 270–287.

[35] Z. Wu, G. Raju, P. Weaver, Framework for the buckling optimization of variable-angle tow composite plates, AIAA Journal 53 (12) (2015) 3788–3804.

[36] S. C. White, P. M. Weaver, Towards imperfection insensitive buckling response of shell structures-shells with plate-like post-buckled responses, The Aeronautical Journal 120 (1224) (2016) 233–253.

[37] R. Groh, P. Weaver, Buckling analysis of variable angle tow, variable thickness panels with transverse shear effects, Composite Structures 107 (2014) 482–493.

[38] B. H. Coburn, P. M. Weaver, Buckling analysis, design and optimisation of variable-stiffness sandwich panels, International Journal of Solids and Structures 96 (2016) 217 – 228.

[39] V. Oliveri, A. Milazzo, A rayleigh-ritz approach for postbuckling analysis of variable angle tow composite stiffened panels, Computers and Structures 196 (2018) 263–276.

[40] V. Oliveri, A. Milazzo, P. Weaver, Thermo-mechanical post-buckling analysis of variable angle tow composite plate assemblies, Composite Structures 183 (1) (2018) 620–635.

[41] G. Sciascia, V. Oliveri, A. Milazzo, P. M. Weaver, Ritz solution for transient analysis of variable-stiffness shell structures, AIAA Journal 58 (4) (2020) 1796–1810.

[42] E. Riks, C. Rankin, F. Brogan, The buckling behavior of a central crack in a plate under tension, Engineering Fracture Mechanics 43 (4) (1992) 529 – 548.

[43] J. Yuan, S. Dickinson, Flexural vibration of rectangular plate systems approached by using artificial springs in the Rayleigh-Ritz method, Journal of Sound and Vibration 159 (1) (1992) 39–55.

[44] K. Liew, K. Hung, M. Lim, A solution method for analysis of cracked plates under vibration, Engineering Fracture Mechanics 48 (1994) 393–404.

[45] T. Dang, R. Kapania, Ritz approach for buckling prediction of cracked-stiffened structures, Journal of Aircraft 50 (3) (2013) 965–974.

[46] A. Milazzo, V. Oliveri, Post-buckling analysis of cracked multilayered composite plates by pb-2 rayleigh-ritz method, Composite Structures 132 (2015) 75–86.

[47] A. Milazzo, V. Oliveri, Buckling and postbuckling of stiffened composite panels with cracks and delaminations by ritz approach, AIAA Journal 55 (3) (2017) 965–980.

[48] S. Ghannadpour, M. Karimi, F. Tornabene, Application of plate decomposition technique in nonlinear and post-buckling analysis of functionally graded plates containing crack, Composite Structures 220 (2019) 158 – 167.

[49] H. Lee, Fundamental frequencies of annular plates with internal cracks, Computers and Structures 43 (6) (1992) 1085–1089.

[50] A. Leissa, O. McGee, C. Huang, Vibrations of circular plates having v-notches or sharp radial cracks, Journal of Sound and Vibration 161 (2) (1993) 227–239.

[51] H. Lee, S. Lim, Vibration of cracked rectangular plates including transverse shear deformation and rotary inertia, Computers and Structures 49 (4) (1993) 715–718.

[52] O. McGee, A. Leissa, C. Huang, J. Kim, Vibrations of circular plates with clamped v-notches or rigidly constrained radial cracks, Journal of Sound and Vibration 181 (2) (1995) 185–201.

[53] V. Ramamurti, S. Neogy, Effect of cracks on the natural frequency of cantilevered plates - a Rayleigh-Ritz solution, Mechanics of Structures and Machines 26 (2) (1998) 131–143.

[54] O. McGee, A. Leissa, J. Kim, Y. Kim, Vibration of plates with constrained v-notches or cracks, Journal of Engineering Mechanics 129 (7) (2003) 812–822.

[55] C. Huang, A. Leissa, Vibration analysis of rectangular plates with side cracks via the Ritz method, Journal of Sound and Vibration 323 (3-5) (2009) 974–988.

[56] C. Huang, A. Leissa, C. Chan, Vibrations of rectangular plates with internal cracks or slits, International Journal of Mechanical Sciences 53 (6) (2011) 436–445.

[57] C. Huang, A. Leissa, R. Li, Accurate vibration analysis of thick, cracked rectangular plates, Journal of Sound and Vibration 330 (9) (2011) 2079–2093.

[58] C. Huang, O. McGee, M. Chang, Vibrations of cracked rectangular FGM thick plates, Composite Structures 93 (7) (2011) 1747–1764.

[59] H. Zeng, C. Huang, A. Leissa, M. Chang, Vibrations and stability of a loaded side-cracked rectangular plate via the MLS-Ritz method, Thin-Walled Structures 106 (2016) 459–470.

[60] A. Milazzo, I. Benedetti, V. Gulizzi, An extended ritz formulation for buckling and post-buckling analysis of cracked multilayered plates, Composite Structures 201 (2018) 980–994.

[61] A. Milazzo, I. Benedetti, V. Gulizzi, A single-domain ritz approach for buckling and post-buckling analysis of cracked plates, International Journal of Solids and Structures 159 (2019) 221–231.

[62] V. Gulizzi, V. Oliveri, A. Milazzo, Buckling and post-buckling analysis of cracked stiffened panels via an x-ritz method, Aerospace Science and Technology 86 (2019) 268–282.

[63] J. Reddy, Mechanics of laminated composite plates and shells. Theory and analysis, CRC Press, 2004.

[64] J. K. Knowles, N.-M. Wang, On the bending of an elastic plate containing a crack, Journal of Mathematics and Physics 39 (1-4) (1960) 223–236.

[65] N. M. Wang, Twisting of an elastic plate containing a crack, International Journal of Fracture Mechanics 6 (4) (1970) 367–378.

[66] F. W Delate, F. Erdogan, The effect of transverse shear in a cracked plate under skew-symmetric loading, ASME-Journal of Applied Mechanics 46 (3) (1979) 618–624.

[67] M. V. V. Murthy, K. N. Raju, S. Viswanath, On the bending stress distribution at the tip of a stationary crack from reissner's theory, International Journal of Fracture 17 (6) (1981) 537–552.

[68] A. T. Zehnder, M. J. Viz, Fracture mechanics of thin plates and shells under combined membrane, bending, and twisting loads, Applied Mechanics Reviews 58 (1) (2005) 37–48.

[69] C. Atkinson, L. Xanthis, M. Bernal, Boundary integral equation crack-tip analysis and applications to elastic media with spatially varying elastic properties, Computer Methods in Applied Mechanics and Engineering 29 (1) (1981) 35 – 49.

[70] F. Delale, F. Erdogan, The Crack Problem for a Nonhomogeneous Plane, Journal of Applied Mechanics 50 (3) (1983) 609–614.

[71] V. Fabrikant, External crack in nonhomogeneous elasticity, Engineering Fracture Mechanics 22 (5) (1985) 855 – 858.

[72] J. W. Eischen, Fracture of nonhomogeneous materials, International Journal of Fracture 34 (1) (1987) 3 – 22.

[73] R. Seifi, N. Khoda-Yari, Experimental and numerical studies on buckling of cracked thin-plates under full and partial compression edge loading, Thin-Walled Structures 49 (12) (2011) 1504–1516.

[74] A. Nasirmanesh, S. Mohammadi, Xfem buckling analysis of cracked composite plates, Composite Structures 131 (2015) 333–343.

[75] G. Clancy, D. Peeters, V. Oliveri, D. Jones, R. M. O'Higgins, P. M. Weaver, A study of the influence of processing parameters on steering of carbon fibre/peek tapes using laser-assisted tape placement, Composites Part B: Engineering 163 (2019) 243–251. doi:https://doi.org/10.1016/j.compositesb.2018.11.033.

[76] G. Clancy, D. Peeters, R. M. O'Higgins, P. M. Weaver, In-line variable spreading of carbon fibre/thermoplastic pre-preg tapes for application in automatic tape placement, Materials & Design 194 (2020) 108967. doi:https://doi.org/10.1016/j.matdes.2020.108967.

[77] R. M. Jones, Mechanics of composite materials, Vol. 193, Scripta book Company Washington, DC, 1975.

Appendix A. VAT laminates stiffness matrices

Assuming a plane stress state, the material behaviour at a composite lamina point with fibre orientation angle ϑ is described by the linear elastic constitutive law expressed in the $x_1x_2x_3$ reference frame. Thus, denoting by the superscript $\langle k\rangle$ quantities referring to the k-th ply of a laminate one writes [77]

$$\boldsymbol{\sigma}^{\langle k\rangle} = \left\{ \begin{array}{c} \boldsymbol{\sigma}_p^{\langle k\rangle} \\ \hline \boldsymbol{\sigma}_n^{\langle k\rangle} \end{array} \right\} = \left\{ \begin{array}{c} \sigma_{11}^{\langle k\rangle} \\ \sigma_{22}^{\langle k\rangle} \\ \sigma_{12}^{\langle k\rangle} \\ \hline \sigma_{31}^{\langle k\rangle} \\ \sigma_{32}^{\langle k\rangle} \end{array} \right\} = \left[\begin{array}{ccc|cc} Q_{11}^{\langle k\rangle} & Q_{12}^{\langle k\rangle} & Q_{13}^{\langle k\rangle} & 0 & 0 \\ Q_{12}^{\langle k\rangle} & Q_{22}^{\langle k\rangle} & Q_{23}^{\langle k\rangle} & 0 & 0 \\ Q_{13}^{\langle k\rangle} & Q_{23}^{\langle k\rangle} & Q_{33}^{\langle k\rangle} & 0 & 0 \\ \hline 0 & 0 & 0 & Q_{44}^{\langle k\rangle} & Q_{45}^{\langle k\rangle} \\ 0 & 0 & 0 & Q_{45}^{\langle k\rangle} & Q_{55}^{\langle k\rangle} \end{array} \right] \left\{ \begin{array}{c} \varepsilon_{11}^{\langle k\rangle} \\ \varepsilon_{22}^{\langle k\rangle} \\ \varepsilon_{12}^{\langle k\rangle} \\ \hline \varepsilon_{31}^{\langle k\rangle} \\ \varepsilon_{32}^{\langle k\rangle} \end{array} \right\} = \tag{A.1}$$

$$\left[\begin{array}{c|c} \boldsymbol{Q}_p^{\langle k\rangle} & \boldsymbol{0} \\ \hline \boldsymbol{0} & \boldsymbol{Q}_n^{\langle k\rangle} \end{array} \right] \left\{ \begin{array}{c} \boldsymbol{\varepsilon}_p^{\langle k\rangle} \\ \hline \boldsymbol{\varepsilon}_n^{\langle k\rangle} \end{array} \right\} = \boldsymbol{Q}^{\langle k\rangle} \boldsymbol{\varepsilon}$$

where, σ_{ij} and ε_{ij} are the stress and strain components and

$$Q_{11}^{\langle k\rangle} = \bar{Q}_{11}^{\langle k\rangle} \cos^4\vartheta + 2\left(\bar{Q}_{12}^{\langle k\rangle} + 2\bar{Q}_{33}^{\langle k\rangle}\right) \sin^2\vartheta \cos^2\vartheta + \bar{Q}_{22}^{\langle k\rangle} \sin^4\vartheta \tag{A.2a}$$

$$Q_{12}^{\langle k\rangle} = \bar{Q}_{12}^{\langle k\rangle} \cos^4\vartheta + \left(\bar{Q}_{11}^{\langle k\rangle} + Q_{22}^{\langle k\rangle} - 4\bar{Q}_{33}^{\langle k\rangle}\right) \sin^2\vartheta \cos^2\vartheta + \bar{Q}_{12}^{\langle k\rangle} \sin^4\vartheta \tag{A.2b}$$

$$Q_{22}^{\langle k\rangle} = \bar{Q}_{11}^{\langle k\rangle} \sin^4\vartheta + 2\left(\bar{Q}_{12}^{\langle k\rangle} + 2\bar{Q}_{33}^{\langle k\rangle}\right) \sin^2\vartheta \cos^2\vartheta + \bar{Q}_{22}^{\langle k\rangle} \cos^4\vartheta \tag{A.2c}$$

$$Q_{13} = \left(\bar{Q}_{11}^{\langle k\rangle} - \bar{Q}_{12}^{\langle k\rangle} - 2\bar{Q}_{33}^{\langle k\rangle}\right) \sin\vartheta \cos^3\vartheta + \left(\bar{Q}_{12}^{\langle k\rangle} - \bar{Q}_{22}^{\langle k\rangle} + 2\bar{Q}_{33}^{\langle k\rangle}\right) \sin^3\vartheta \cos\vartheta \tag{A.2d}$$

$$Q_{23} = \left(\bar{Q}_{11}^{\langle k\rangle} - \bar{Q}_{12}^{\langle k\rangle} - 2\bar{Q}_{33}\right)^{\langle k\rangle} \sin^3\vartheta \cos\vartheta + \left(\bar{Q}_{12}^{\langle k\rangle} - \bar{Q}_{22}^{\langle k\rangle} + 2\bar{Q}_{33}\right)^{\langle k\rangle} \sin\vartheta \cos^3\vartheta \tag{A.2e}$$

$$Q_{33} = \left(\bar{Q}_{11}^{\langle k\rangle} + \bar{Q}_{22}^{\langle k\rangle} - 2\bar{Q}_{12}^{\langle k\rangle} - 2\bar{Q}_{33}^{\langle k\rangle}\right) \sin^2\vartheta \cos^2\vartheta + \bar{Q}_{33}{}^{\langle k\rangle} \left(\sin^4\vartheta + \cos^4\vartheta\right) \tag{A.2f}$$

$$Q_{44}^{\langle k\rangle} = \bar{Q}_{44}^{\langle k\rangle} \cos^2\vartheta + \bar{Q}_{55}^{\langle k\rangle} \sin^2\vartheta \tag{A.2g}$$

$$Q_{45}^{\langle k\rangle} = \left(\bar{Q}_{55}^{\langle k\rangle} - \bar{Q}_{44}^{\langle k\rangle}\right) \cos\vartheta \sin\vartheta \tag{A.2h}$$

$$Q_{55}^{\langle k\rangle} = \bar{Q}_{44}^{\langle k\rangle} \sin^2\vartheta + \bar{Q}_{55}^{\langle k\rangle} \cos^2\vartheta \tag{A.2i}$$

In the Eq. (A.2), the $\bar{Q}_{ij}$ are the ply stiffness coefficients in the material reference system that are given by

$$\bar{Q}_{11}^{\langle k\rangle} = \frac{E_1^{\langle k\rangle}}{1-\nu_{12}^{\langle k\rangle}\nu_{21}^{\langle k\rangle}} \tag{A.3a}$$

$$\bar{Q}_{22}^{\langle k\rangle} = \frac{E_2^{\langle k\rangle}}{1-\nu_{12}^{\langle k\rangle}\nu_{21}^{\langle k\rangle}} \tag{A.3b}$$

$$\bar{Q}_{12}^{\langle k\rangle} = \frac{\nu_{12}^{\langle k\rangle}E_2^{\langle k\rangle}}{1-\nu_{12}^{\langle k\rangle}\nu_{21}^{\langle k\rangle}} \tag{A.3c}$$

$$\bar{Q}_{33}{}^{\langle k\rangle} = G_{12}^{\langle k\rangle} \tag{A.3d}$$

$$\bar{Q}_{44}^{\langle k\rangle} = G_{13}^{\langle k\rangle} \tag{A.3e}$$

$$\bar{Q}_{55}{}^{\langle k\rangle} = G_{23}^{\langle k\rangle} \tag{A.3f}$$

where $E_1^{\langle k\rangle}$ ed $E_2^{\langle k\rangle}$ are the Young moduli, $G_{ij}^{\langle k\rangle}$ are the shear moduli and $\nu_{ij}^{\langle k\rangle}$ are the Poisson's coefficients.

For a laminate consisting of N_L layers, the extensional, bending–extensional, bending and shear stiffness matrices are respectively defined as [63]

$$\boldsymbol{A} = \sum_{k=1}^{N_L}\int_{h_{k-1}}^{h_k} \boldsymbol{Q}_p^{\langle k\rangle}\,dx_3 \tag{A.4a}$$

$$\boldsymbol{B} = \sum_{k=1}^{N_L}\int_{h_{k-1}}^{h_k} x_3\boldsymbol{Q}_p^{\langle k\rangle}\,dx_3 \tag{A.4b}$$

$$\boldsymbol{D} = \sum_{k=1}^{N_L}\int_{h_{k-1}}^{h_k} x_3^2\boldsymbol{Q}_p^{\langle k\rangle}\,dx_3 \tag{A.4c}$$

$$\boldsymbol{S} = \sum_{k=1}^{N_L}\int_{h_{k-1}}^{h_k} \boldsymbol{Q}_n^{\langle k\rangle}\,dx_3 \tag{A.4d}$$

being h_{k-1} and h_k the x_3 coordinate of the k-th ply bottom and top faces, respectively.

For VAT composite, the fibre orientation angle varies within each layer as a function of the in-plane coordinates, namely $\vartheta = \vartheta(x_1, x_2)$. Consequently, in VAT laminates the extensional stiffness matrix $\boldsymbol{A}$, the bending–extensional stiffness matrix $\boldsymbol{B}$, the bending stiffness matrix $\boldsymbol{D}$ and the shear stiffness matrix $\boldsymbol{S}$ are function of the plate in-plane coordinates x_1 and x_2